Journal of Geochemical Exploration 158 (2015) 95–111

Contents lists available at ScienceDirect

Journal of Geochemical Exploration

journal homepage: www.elsevier.com/locate/jgeoexp

TEM observations of particles based on sampling in gas and soil at the Dongshengmiao polymetallic pyrite deposit, Inner Mongolia, Northern China

Songying Luo [a], Jianjin Cao [a,b,*], Hongbin Yan [a], Jie Yi [a]

[a] Department of Earth Science, Sun Yat-sen University, Guangzhou 510275, China
[b] Guangdong Provincial Key Laboratory of Geological Process and Mineral Resources Survey, Guangzhou 510275, China

ARTICLE INFO

Article history:
Received 15 May 2015
Accepted 14 July 2015
Available online 18 July 2015

Keywords:
Ascending gas flow
Elemental association
Concealed deposit
Transmission electron microscopy

ABSTRACT

Forty-two samples of particles that were carried by the ascending gas flow and forty-two corresponding soil samples were captured from Quaternary sediments overlying the Dongshengmiao polymetallic pyrite deposit in the Province of Inner Mongolia, North China. The category, size, shape, chemical composition and structure of these particles were analyzed by transmission electron microscopy (TEM) technique. The observations indicated that most of the particles carried by the ascending gas flow were sub-circular, elliptical or irregular in shape, with sizes ranging from 5 nm to 400 nm; their primary components were dominated by the metallogenic elements Fe, Cu, Zn and Pb, and their highest weight percentages were up to 80.2%, 82.5%, 49.1% and 59.6%, respectively. We determine that a large number of metal sulfides and oxides/hydroxides (such as PbS, Fe_3O_4, Sb_3O_2 and $Fe(OH)_3$), native metal alloy (such as native vanadium–platinum–iron–cobalt alloy), nonmetallic oxides (such as SiO_2), chlorides (primarily NaCl), nonmetallic hydroxides (such as KOH) and sulfate (primarily $BaSO_4$) particles, as well as precious metal elements (such as Au and Pt) bearing particles and rare earth elements (such as Y) as observed in the samples, exhibited a good correspondence with the concealed ore bodies and the wall rock. A number of the particles that were carried by the ascending gas flow were found in elemental associations S–Cu, S–Zn, S–Pb, S–Mo, S–Fe–Zn, S–Fe–Cu, S–Fe–Cu–Mo, S–Fe–Zn–Pb and Cr–Mn–Fe, which were consistent with previous studies on the mineral assemblages of this deposit. The particles carried by the ascending gas flow and soil particles have a common origin, that is, the ore body. Different particles carried by ascending gas flows come from different types of deposits, without interference from the properties or thickness of the overlying layer, suggesting that geogas prospecting could be used to explore for different types of ore deposits. An analysis of the particles carried by the ascending gas flow along the 14th exploration line demonstrates a good spatial correlation with the known concealed ore bodies. Additionally, Pt-bearing and rare earth element bearing particles were first found in the ascending gas flow from the Dongshengmiao deposit.

© 2015 Elsevier B.V. All rights reserved.

1. Introduction

Geogas prospecting is a relatively new technique that was first proposed by Kristiansson and Malmqvist in the early 1980s and is aimed at breaking through difficult prospecting bottlenecks to locate deep-seated and concealed mineral deposits (Kristiansson and Malmqvist, 1982, 1987; Kristiansson et al., 1990; Malmqvist and Kristiansson, 1981, 1984; Malmqvist et al., 1999). The basic principles of geogas prospecting are that geogas is widely present as an ascending gas flow in the earth (Gold and Soter, 1980; Chiodini et al., 1995; Xie, 1995; Wang et al., 1997; Tong and Li, 1999; Wang et al., 1999; Morner and Etiope, 2002; Etiope and Martinelli, 2002; Annunziatellis et al., 2003; Wang, 2003; Cameron et al., 2004; Wang et al., 2007) and when the ascending gas flows through the ore body, it can carry solid substances from the concealed ore bodies or other geological bodies and transport them to the earth's surface; these solid substances primarily take the form of nano-scale particles (Cao, 2011; Cao et al., 2010a; Etiope, 1998; Etiope and Lombardi, 1996; Tong and Li, 1999; Tong et al., 1998; Wang et al., 2007). These ascending gas flow-carried substances can be captured by a collector, and a wealth of mineralization information about the concealed ore bodies can be obtained by using modern testing technologies (Cao et al., 2005, 2009, 2010b; Ma et al., 1998; Malmqvist et al., 1999; Tong and Li, 1999; Tong et al., 1998; Wang et al., 1997, 1999, 2007; Xie et al., 1999).

Currently, increasing numbers of scholars are paying attention to geogas prospecting technology. This technology is based on decades of development, and it is primarily embodied in the development of key techniques, including sampling methods, trapping mediums and analysis techniques. The current geogas sampling methods are primarily the static method and the dynamic method (Kristiansson et al., 1990; Malmqvist et al., 1999; Wang et al., 1997; Xie et al., 1999). The trapping mediums are comprised of various adsorption materials, for example,

* Corresponding author at: Department of Earth Science, Sun Yat-sen University, Guangzhou 510275, China.
E-mail address: eescjj@mail.sysu.edu.cn (J. Cao).

http://dx.doi.org/10.1016/j.gexplo.2015.07.007
0375-6742/© 2015 Elsevier B.V. All rights reserved.

plastic film, polyurethane foam plastics, activated carbon and liquid adsorption materials (Kristiansson et al., 1990; Malmqvist et al., 1999; Pauwels et al., 1999; Tong et al., 1998). The analysis techniques include particle-induced X-ray emission (PIXE) (Kristiansson et al., 1990; Malmqvist et al., 1999), resonance ionization mass spectrometry (RIMS) (Ma et al., 1997), laser single atom detection (LSAD) (Wang et al., 1997), laser excited atomic fluorescence spectrometry (LEAFS) (Ma et al., 1998), instrumental neutron activation analysis (INAA) (Tong and Li, 1999; Wang et al., 1997), and inductively coupled plasma mass spectrometry (ICP-MS) (Pauwels et al., 1999).

However, the traditional geogas prospecting methods only estimated the elemental concentrations of the geogas matter but cannot detect their morphological characteristics. Tong et al. (1998) used atomic force microscopy (AFM), scanning electron microscopy (SEM) and transmission electron microscopy (TEM) to observe the geogas matter, and they demonstrated that the geogas matter is transported in the form of nano-scale particles. Because of the technological restrictions at that time, those analytical techniques can only be used to observe the morphology of a pile of nano-particles because the low resolution and oxygen elements cannot be measured. Cao (2009) proposed using high resolution transmission electron microscopy (HRTEM) to observe a single particle in the ascending gas flow, combining the particle characteristics with the elemental concentrations in the particles to determine the concealed deposits. In comparison with other analysis methods, HRTEM has the advantage of measuring the low-value anomaly on geogas matter because of its high sensitivity, and it is used to observe the morphology and structure of a single nano-particle because of its high resolution. In our work, we attempt to analyze the particles carried by the ascending gas flow in a new way, that is, not only to estimate the composition of the particles but also to deduce the ore minerals and the type of concealed ore bodies by analyzing the morphology, composition, structure and elemental association characteristics on a single particle by HRTEM. We focus on the elemental association characteristics and the spatial relation between the particles that were carried by the ascending gas flow and the concealed ore bodies. On the basis of other analyses of the particles carried by ascending gas flows, an elemental association and abundance characteristic analysis may be more accurate for determining the underground ore body type and may even further determine the genetic deposit types. Our results may be useful for locating concealed ore bodies and promising applications for ore mineralogy exploration.

To collect the particles carried by the ascending gas flow, the nickel grids for TEM were placed directly in Quaternary sediments overlying the Dongshengmiao concealed deposit. Using TEM, we analyzed the category, size, shape, chemical composition and structure of the particles carried by the ascending gas flow. We also discussed the elemental association characteristics and their origins of these particles, the difference between these particles and the corresponding soil particles and then contrasted these particles with that of the characteristics of other concealed deposits. Next, we determined the spatial relationships between the particles carried by the ascending gas flow and the concealed ore bodies.

2. Geological setting

The Dongshengmiao polymetallic pyrite deposit is a super-large deposit, and is one of the best-known deposits in the Langshan belt in Inner Mongolia Province, North China (Fig. 1) (Xia, 1992). Not only are the pyrite reserves first in the nation, but the zinc, lead, copper reserves also reach very large, large and medium sizes, respectively. There is good resource and prospecting potential here because of the large range of mineralization in this region. The exposed strata in the Dongshengmiao area are the Middle Proterozoic Langshan Group, the Mesozoic Lisangou formation, the Tertiary, and the Quaternary. The Langshan Group is a set of clastic sedimentary metamorphic rocks with minor carbonate rocks and ore formation, and it can be further divided into the lower, middle and upper units (Peng et al., 2007). The lower unit is divided into two rock sections, which consist of two-mica quartz schist, sericite quartz schist and quartz conglomerate. The middle unit is divided into five rock sections, which consist of dolomitic-marble, quartzite, schist, graphite sericite schist, two-mica quartz schist and carbon phyllite. The upper unit is divided into two rock sections, which consist of quartzite, mica quartz schist, graphite sericite schist, two-mica quartz schist, sericite quartz schist and dolomitic-marble (Peng and Zhai, 2004; Xia, 1992). The Mesozoic Lisangou formation is primarily characterized by conglomerate and sandstone, including a thin layer of clay rock between them. The Tertiary and Quaternary are primarily composed of sand and gravel. The ore bodies are primarily contained in the middle units of the Langshan Group, which is poorly exposed (Peng et al., 2007). It is generally considered to be a sedimentary exhalative (SEDEX) deposit that is buried at a depth of over four hundred meters to several kilometers (Peng and Zhai, 2004). The style of mineralization and the geological characteristics of the Dongshengmiao deposit are somewhat similar to the well-known SEDEX deposit in which the metallogenic elements were present as S–Cu, S–Cu–Zn, and S–Fe–Pb–Zn in the vertical profile and S–Cu–Pb, S–Pb–Zn, S–Zn, and S–Fe in the horizontal direction (Peng and Zhai, 2004; Xia, 1992), such as the McArthur River deposit (Patrick, 1998a,b) and the Mount Isa deposit (Perkins and Bell, 1998). The primary ore body is controlled by the formation lithology characteristics, which are horizontal, tilt or fold layered and lenticular rich sulfide ore bodies, as well as the management control by a tectonic slice stratiform zinc-rich ore body (Peng and Zhai, 2004; Xia, 1992; Zhang et al., 2010). The metallic minerals in the Dongshengmiao deposit are pyrite, pyrrhotite, sphalerite, siderite, galena, chalcopyrite, marcasite and magnetite. The gangue minerals are dolomite, calcite, quartz, mica and graphite. Zn, Pb and Cu are the major metallic elements in the ore, and there are also some associated elements, such as S, Ag, Co, Ge, Cd, As, F and C (Peng and Zhai, 2004; Peng et al., 2007; Xia, 1992; Zhang et al., 2010). The Langshan Mountain-front fault passed through the Dongshengmiao deposit. This deposit is bound by the F1 fault to the south and the F5 fault to the northeast, which are northeast regional fractures. Most of the deposit area is covered by Cretaceous sediments. It is only exposed within a limited area of the deposit (Peng et al., 2007).

3. Sampling and analytical method

We used the static method to collect the particles that were carried by the ascending gas flow. The sampling points were distributed along the 14th exploration line (Fig. 1), where the ore bodies of the Dongshengmiao deposit were concentrated and exhibited large thicknesses. The samples were collected along the prospecting line every 50 m such that 42 samples were collected. Our sampling device has been improved on the basis of previous work (Cao et al., 2009, 2010b; Kristiansson et al., 1990; Malmqvist et al., 1999; Wei et al., 2013). The sampling device (Fig. 2) consists of a simple plastic funnel, a carbon-coated nickel TEM grid, a plastic film, two nylon nets, a plastic cup, a silica gel plug, a hard plastic tube and a small plastic tube. This sampling method is similar to that of Wei et al. (2013), except that a silica gel plug is placed inside the small opening of the funnel, and a small plastic tube with a TEM grid fixed by two nylon nets is placed into the silica gel plug to improve the adsorption rate.

The particles carried by the ascending gas flow collected in this deposit were analyzed by TEM (Tecnai G2 F30 S-Twin, America) and energy dispersive X-ray spectrometer (EDS) (EDXA, America) at a maximum accelerating voltage of 300 kV. The TEM analyses were performed at the Instrument Analysis Center of Yangzhou University. Because the grids were made with carbon-coated and nickel, we eliminated the carbon and nickel content from the analyses. Forty-one nickel TEM girds were observed and photographed (one grid was contaminated), and EDS

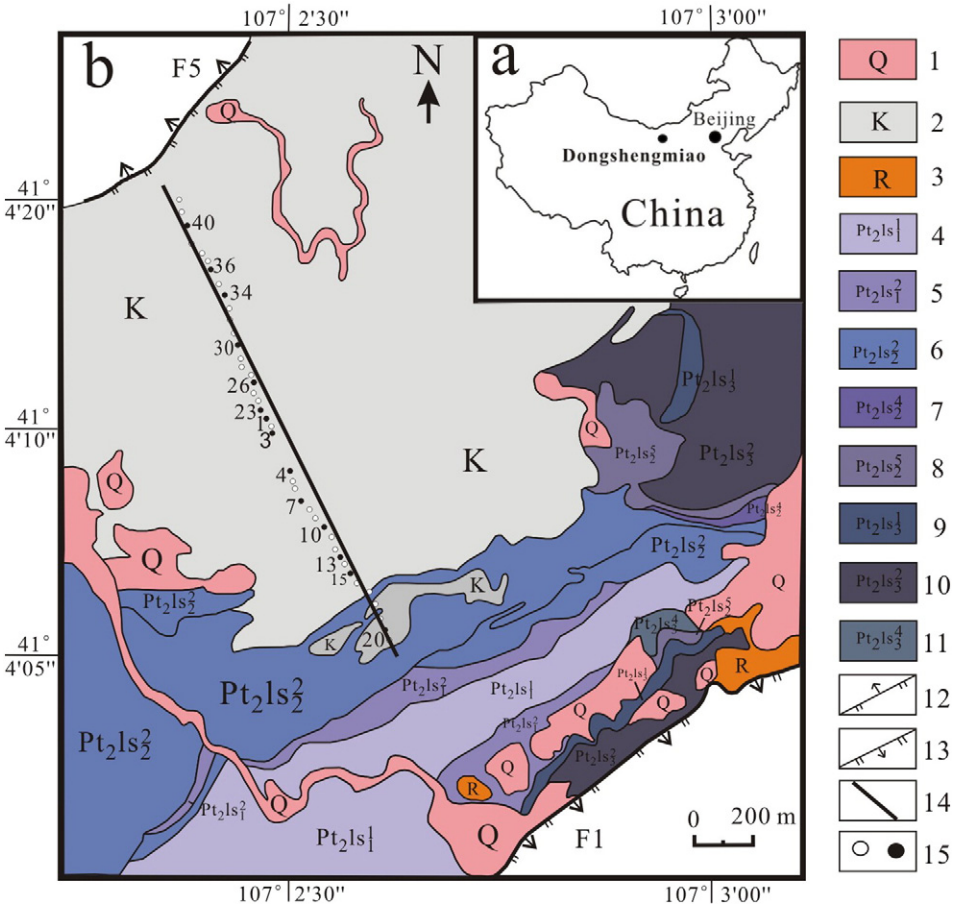

Fig. 1. Position of sampling points and schematic geological map of Dongshengmiao polymetallic pyrite deposit (modified according to the map provided by Dongshengmiao Mineral Company Limited). 1 — Quaternary sediments, 2 — Cretaceous red glutenite, 3 — Tertiary glutenite, 4 — the First rock member of the Lower fm of the Mesoproterozoic Langshan Group, 5 — the Second rock member of the Lower fm of the Mesoproterozoic Langshan Group, 6 — the Second rock member of the Middle fm of the Mesoproterozoic Langshan Group, 7 — the Fourth rock member of the Middle fm of the Mesoproterozoic Langshan Group, 8 — the Fifth rock member of the Middle fm of the Mesoproterozoic Langshan Group, 9 — the First rock member of the Upper fm of the Mesoproterozoic Langshan Group, 10 — the Second-rock member of the Upper fm of the Mesoproterozoic Langshan Group, 11 — the Fourth-rock member of the Upper fm of the Mesoproterozoic Langshan Group, 12 — normal fault, 13 — reversed fault, 14 — sampling line, and 15 — sampling points.

and selected area electron diffraction (SAED) or HRTEM image were used to analyze the composition and the crystal structure. The corresponding soil particle samples were collected in holes that were 50 cm deep at each sampling point, and the samples were also analyzed by TEM technique. The corresponding soil samples were sieved under less than 400 mesh after drying at room temperature (Wang et al., 2012). The scattered samples were blown up by washing-ear-ball in the beaker, and they were then allowed to fall on TEM grids.

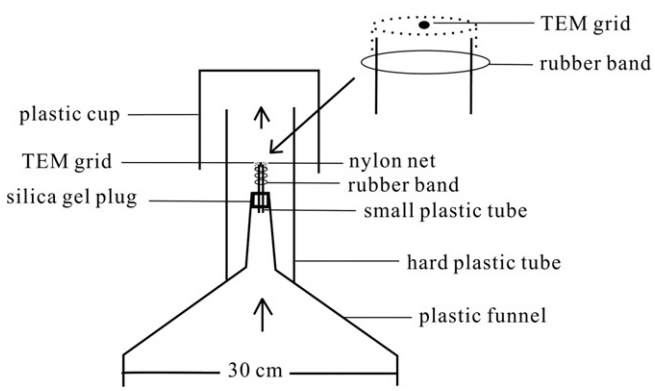

Fig. 2. Sketch of the collector used for particles carried by the ascending gas flow.

4. Results

4.1. Particles carried by the ascending gas flow from the Dongshengmiao deposit

In our work, 42 TEM grid samples were collected and 122 particles were analyzed. The typical particles are as follows.

4.1.1. The metallogenic element-bearing particles

A large number of particles containing metallogenic elements (such as Fe, Cu, Zn and Pb) were observed with a TEM. The particles were usually observed in elemental associations (such as S–Fe–Zn, S–Fe–Cu, S–Fe–Cu–Mo, S–Fe–Zn–Pb, S–Zn–Pb and Cr–Mn–Fe). In addition, a number of Mo and Sb oxide particles were observed. We divided these particles into several types according to the component and the morphology.

(1) Iron oxide and hydroxide particles: Fe is widely observed in our samples, and its concentrations in the Fe-bearing particles primarily ranged from 40% to 60%, with up to 80.2%. An approximately elliptical Fe-bearing particle (ID: 1) with a 50 nm short radius was observed, and there is a smaller sub-circular particle above it, with an approximately 25 nm diameter (Fig. 3). The particles were composed of O (27.1%) and Fe (72.3%), with minor amounts of Si (0.5%) (Table 1). The atom percentages suggest that they may be Fe_3O_4 containing little SiO_2.

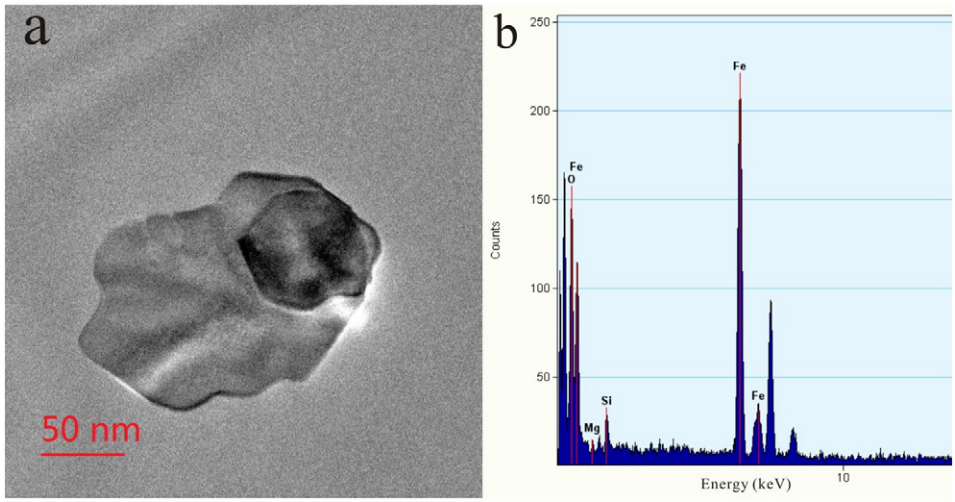

Fig. 3. Fe-bearing particles. (a) TEM image. (b) EDS results.

A number of Fe-bearing particles were in observed as S–Fe–Zn. This type of particle was observed 24 times in our samples. An elliptical assemblage of S–Fe–Zn bearing particles (ID: 2) at 100 nm in diameter was observed (Fig. 4-a). The primary components of the particles (Table 1) are O (42.6%), Fe (49.0%) and Zn (2.4%), including minor amounts of Na (1.1%), Si (1.6%), P (0.4%), S (0.9%), Cl (0.9%) and Ca (1.3%). The SAED result revealed that it is polycrystalline. The lattice fringes of the individual could be clearly observed in the HRTEM image, indicating that the particles are well crystallized. The distance between the two adjacent planes in the HRTEM image is 0.252 nm. Without considering the H content that cannot be determined by using the X-ray energy spectrum, the HRTEM image and atom percentages suggest that the particle may be $Fe(OH)_3$, with a small quantity of Zn-bearing particles and impurities.

Some of the Fe-bearing particles were present as Cr–Mn–Fe. This type of particle was observed 26 times in this study. There was an approximately circular particle (ID: 3) (Fig. 4-b) that was approximately 200 nm in diameter and composed of O (6.2%), Si (0.5%), Cr (19.5%), Mn (2.9%) and Fe (70.9%) (Table 1). Several clear diffraction rings that were doped with spots were recorded and shown in a pattern, suggesting crystalline oxide particles of Cr, Mn and Fe.

(2) Cu-bearing particles: 17 of the O–S–Cu-bearing particles (ID: 4) (Fig. 5) exhibited similar appearances and components, albeit with different weight percentages. The particles sizes are ranged from 5 nm to 50 nm. One of the EDS analysis results (Table 1) revealed that the primary components of the particles are O (11.2%), S (19.2%) and Cu (69.6%), and their atomic ratio is close to 1:1:2. The distance between the two adjacent planes in the HRTEM image is 0.195 nm, suggesting that the aggregated particles are crystalline sulfide or Cu oxide.

A number of Cu-bearing particles were observed as S–Fe–Cu or S–Fe–Cu–Mo. This type of particle was observed 16 times in the samples. An irregular assemblage of S–Fe–Cu-bearing particles (ID: 5) with a size of 200 nm × 500 nm was observed (Fig. 6). The particles (Table 1) are composed of S (25.3%), Fe (30.4%) and Cu (38.6%), including minor amounts of O (4.9%) and Si (0.8%). Discontinuous diffraction rings were made up of many diffraction spots and shown in the SAED pattern, suggesting that there may be some crystalline particles of S, Cu and Mo.

(3) Mo-bearing particles: A sub-circular Mo-bearing particle (ID: 6) with a size of approximately 200 nm was observed (Fig. 7-a). The primary components of the particle (Table 1) are O (44.5%) and Mo (41.9%), including minor amounts of Al (0.3%), Si (1.8%), S (5.6%), Ca (2.5%) and Fe (3.3%). The diffraction rings and HRTEM image are not clear, suggesting that the particle is non-crystalline.

(4) Zn-bearing particles: A circular Zn-bearing particle (ID: 7) with a diameter of 100 nm was observed (Fig. 7-b). The primary components of the particle (Table 1) are O (18.1%), Si (0.7%), S (20.6%), Cl (6.3%), K (2.0%), Ca (3.2%) and Zn (49.1%). The HRTEM image indicated that the particles are composed of many small crystals, each of which has different crystal orientations, with some of

Table 1
EDS results for the particles carried by the ascending gas flow (1–8).

Element	Particle number							
	1	2	3	4	5	6	7	8
Weight_O (%)	27.13	42.55	6.21	11.18	4.86	44.53	18.07	12.18
Atomic_O (%)	56.34	70.48	18.47	29.21	13.36	77.46	39.53	36.51
Weight_F (%)								
Atomic_F (%)								
Weight_Na (%)		1.1						1.59
Atomic_Na (%)		1.27						3.32
Weight_Al (%)						0.3		
Atomic_Al (%)						0.31		
Weight_Si (%)	0.53	1.6	0.46		0.75	1.81	0.67	0.29
Atomic_Si (%)	0.63	1.51	0.79		1.18	1.79	0.83	0.51
Weight_P (%)		0.36						
Atomic_P (%)		0.31						
Weight_S (%)		0.88		19.19	25.34	5.59	20.64	10.08
Atomic_S (%)		0.73		25.01	34.77	4.85	22.53	15.08
Weight_Cl (%)		0.85					6.27	
Atomic_Cl (%)		0.63					6.19	
Weight_K (%)							1.98	26.34
Atomic_K (%)							1.77	32.3
Weight_Ca (%)		1.25				2.53	3.24	
Atomic_Ca (%)		0.82				1.75	2.83	
Weight_Cr (%)			19.5					
Atomic_Cr (%)			17.83					
Weight_Mn (%)			2.93					
Atomic_Mn (%)			2.53					
Weight_Fe (%)	72.33	49.01	70.88		30.44	3.3		1.3
Atomic_Fe (%)	43.02	23.25	60.35		23.97	1.64		1.11
Weight_Cu (%)				69.61	38.58			
Atomic_Cu (%)				45.76	26.7			
Weight_Zn (%)		2.35					49.1	
Atomic_Zn (%)		0.95					26.28	
Weight_Mo (%)						41.9		
Atomic_Mo (%)						12.15		
Weight_Pb (%)								48.18
Atomic_Pb (%)								11.14

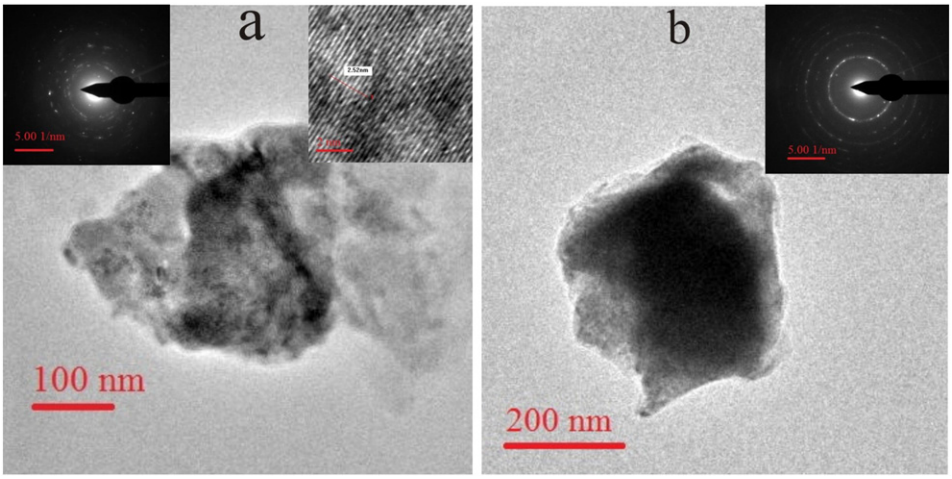

Fig. 4. TEM photomicrograph of Fe-bearing particles. (a) $Fe(OH)_3$ particle. (b) Cr–Mn–Fe particle.

them being well-defined crystals. The SAED and the HRTEM image suggest that the particles may be crystalline oxides or Zn sulfate, which contain some chloride and other oxides.

(5) Pb-bearing particles: An irregular assemblage of particles (ID: 8) with a size of 200 nm × 300 nm was observed (Fig. 8-a). The primary components (Table 1) of the particles are O (12.2%), S (10.1%), K (26.3%) and Pb (48.2%), with minor amounts of Na (1.6%), Si (0.3%) and Fe (1.3%). A clear diffraction ring with regular spots were shown in a pattern, and the clear lattice fringes of the partial region in the HRTEM image suggest that the particles contain some polycrystalline material and some the other phases of single crystal material. The distance between two adjacent planes in the HRTEM image is 0.291 nm, suggesting that the particles contain PbS. The atom percentages and the SAED result suggest that the particles are primarily PbS and KOH, with a small quantity of oxides.

An irregular assemblage of particles (ID: 9) was observed to be 100 nm in diameter (Fig. 8-b). The primary components of the particles (Table 2) are K (18.7%), Zn (13.5%) and Pb (42.9%), including minor amounts of O (8.7%), Na (9.4%), Si (0.3%) and S (6.4%). The lattice fringes of the partial region could be clearly observed in the HRTEM image, indicating that the particles are partly well crystallized. Diffraction rings doped with spots were recorded and shown in a pattern, suggesting crystalline oxide particles of Zn and Pb.

(6) Antimony oxide particles: A polycrystalline Sb-bearing particle (ID: 10) (Fig. 9) with a 50 nm diameter is composed of O (18.1%) and Sb (81.3%), with minor amounts of Na (0.1%) and Si (0.6%) (Table 2). The atomic ratio of Sb to O is close to 1.5 (62.04/36.66 ≈ 1.69), and the distance between the two adjacent planes in the HRTEM image is 0.333 nm, suggesting that the particles are Sb_3O_2.

4.1.2. Precious metal element-bearing particles

Elongated Pt-bearing particles (ID: 11) with a size of 100 nm × 500 nm were observed (Fig. 10). The primary components (Table 2) of the particles are O (17.6%), Fe (12.5%) and Pt (59.6%), with minor amounts of Al (1.1%), Si (2.0%) and Co (7.2%). The diffraction rings are broadened, suggesting that the particles are composed of many nanocrystals.

An irregular assemblage of gold-bearing particles (ID: 12) with a size of over 500 nm was observed (Fig. 11). The primary components (Table 2) of the particles are O (44.4%) and Au (35.7%), with minor

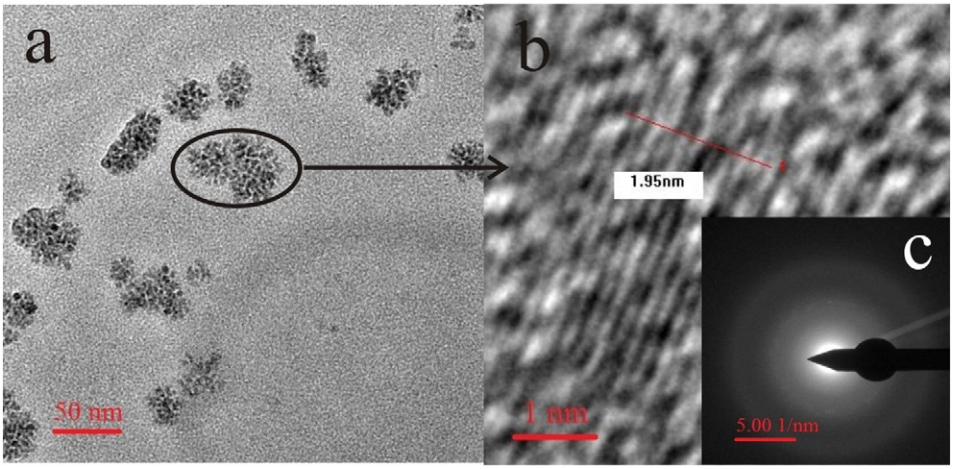

Fig. 5. O, S, and Cu-bearing particles. (a) TEM image. (b) HRTEM image. (c) SAED pattern.

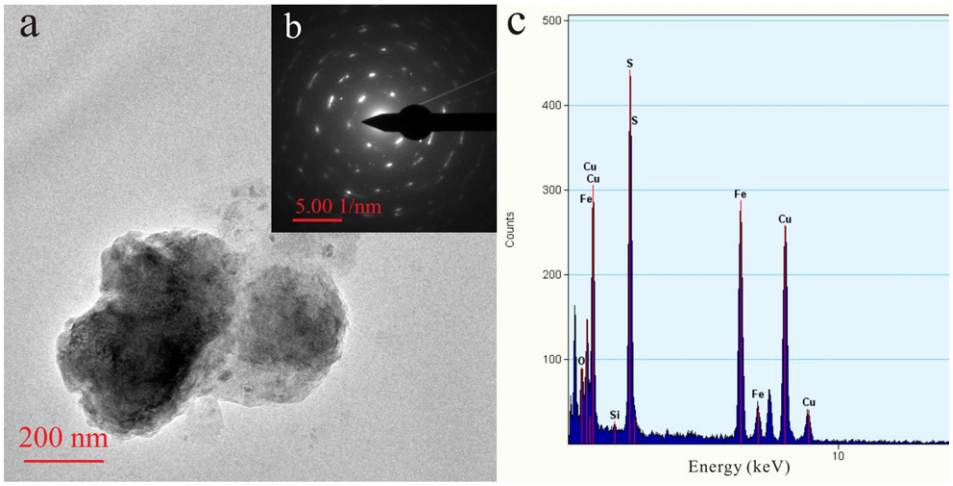

Fig. 6. S, Fe, and Cu-bearing particles. (a) TEM image. (b) SAED pattern. (c) EDS results.

amounts of Mg (0.5%), Al (2.6%), Si (5.5%), Ca (2.2%) and Fe (9.1%). The SAED result indicated that the particles are polycrystalline, and the distance between the two adjacent planes in the HRTEM image is 0.231 nm, suggesting that the particle may be native gold with some oxides.

4.1.3. Rare earth element-bearing particles

A sub-circular assemblage of Y-bearing particles (ID: 13) with a 100 nm diameter was observed (Fig. 12-a). The primary components of the particles (Table 2) are O (38.1%), P (17.2%) and Y (40.0%), including minor amounts of Na (1.5%), Si (1.1%) and Cu (2.1%). Many diffraction spots were irregularly distributed, suggesting the particles may be polycrystalline. The atomic percentage and the SAED result suggest that the particles may be Y[PO_4], including some oxides.

4.1.4. Native metal alloy particles

An elongated particle (ID: 14) with a size of 50 nm × 100 nm (Fig. 12-b) is composed of V (1.4%), Fe (43.6%), Co (48.9%) and Pt (6.1%) (Table 2). The diffraction rings are broadened, suggesting that the particle is composed of many nano-crystals. The composition and the SAED result suggest that the particle is a native vanadium–platinum–iron–cobalt alloy.

4.1.5. Sulfate and chloride particles

A circular assemblage of particles (ID: 15) with a 100 nm diameter was observed (Fig. 13-a). The primary components of the particles (Table 2) are O (42.1%), S (11.1%) and Ba (43.5%), with minor amounts of Na (0.3%), Si (0.1%), Ca (2.2%) and Ti (0.6%). The SAED result indicated that the particles are polycrystalline. The atomic percentages and the distance between two adjacent planes in the HRTEM image was 0.315 nm, suggesting that the particles are $BaSO_4$ containing a small amount of oxides.

A subhedral particle (ID: 16) with a size of 200 nm × 300 nm was observed (Fig. 13-b). The primary components of this particle (Table 2) are Na (40.6%) and Cl (48.0%), with minor amounts of O (7.3%), F (2.6%), Si (0.6%), S (0.6%) and Ca (0.4%). Several clear diffraction rings doped with regular array spots were recorded and shown in a pattern, suggesting that the particle may be a single crystal that is partly destroyed to make polycrystalline. The atomic ratio of Na to Cl is close to 1 (46.97/36.03 ≈ 1.3). The morphology, the diffraction pattern and the atomic percentages, suggest that the particle is NaCl that contains a small amount of impurities.

4.2. The soil particles from the Dongshengmiao deposit

Over 95% of the soil particles were Si, Ca, Ti, and Fe oxides, and a few of were Na, Mg and Al oxides. There were primarily SiO_2, TiO_2, CaO,

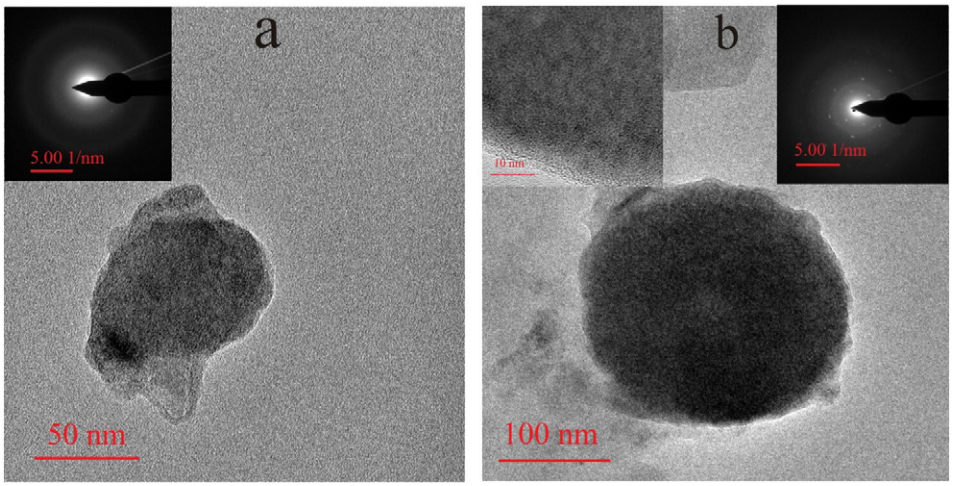

Fig. 7. TEM photomicrograph of (a) Mo-bearing particles and (b) Zn-bearing particles.

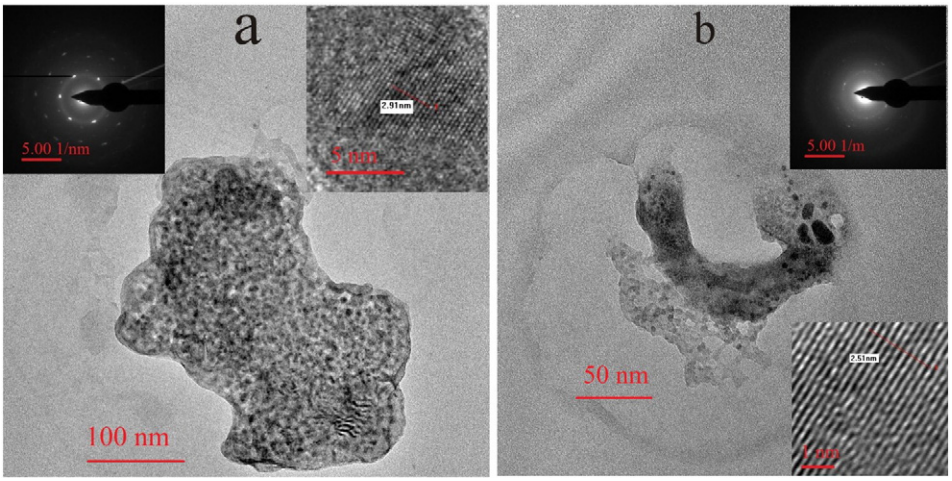

Fig. 8. TEM photomicrograph of (a) Pb-bearing particles and (b) Zn and Pb-bearing particles.

Table 2
EDS results for the particles carried by the ascending gas flow (9–16).

Element	Particle number							
	9	10	11	12	13	14	15	16
Weight_O (%)	8.68	18.07	17.6	44.35	38.02		42.09	7.26
Atomic_O (%)	26.39	62.04	59.06	79.51	67.49		77.82	12.07
Weight_F (%)								2.63
Atomic_F (%)								3.68
Weight_Na (%)	9.39	0.07			1.51		0.31	40.59
Atomic_Na (%)	19.88	0.17			1.86		0.41	46.97
Weight_Mg (%)				0.5				
Atomic_Mg (%)				0.6				
Weight_Al (%)			1.12	2.64				
Atomic_Al (%)			2.22	2.81				
Weight_Si (%)	0.33	0.57	1.95	5.54	1.12		0.08	0.45
Atomic_Si (%)	0.57	1.11	3.74	5.66	1.13		0.09	0.43
Weight_P (%)					17.19			
Atomic_P (%)					15.76			
Weight_S (%)	6.39						11.14	0.64
Atomic_S (%)	9.7						10.28	0.53
Weight_Cl (%)								48.01
Atomic_Cl (%)								36.03
Weight_K (%)	18.71							
Atomic_K (%)	23.29							
Weight_Ca (%)				2.2			2.18	0.39
Atomic_Ca (%)				1.57			1.61	0.26
Weight_Ti (%)							0.64	
Atomic_Ti (%)							0.39	
Weight_V (%)						1.43		
Atomic_V (%)						1.68		
Weight_Fe (%)			12.47	9.02		43.57		
Atomic_Fe (%)			11.98	4.63		46.74		
Weight_Co (%)			7.2			48.87		
Atomic_Co (%)			6.56			49.68		
Weight_Cu (%)					2.11			
Atomic_Cu (%)					0.94			
Weight_Zn (%)	13.5							
Atomic_Zn (%)	10.1							
Weight_Y (%)					40.03			
Atomic_Y (%)					12.78			
Weight_Sb (%)		81.28						
Atomic_Sb (%)		36.66						
Weight_Ba (%)							43.52	
Atomic_Ba (%)							9.37	
Weight_Pt (%)			59.63			6.12		
Atomic_Pt (%)			16.4			1.87		
Weight_Au (%)				35.71				
Atomic_Au (%)				5.2				
Weight_Pb (%)	42.94							
Atomic_Pb (%)	10.08							

$CaSO_4$ and FeO particles; some particles contained a small amount of As, Hg or Zn.

(1) Oxide particles

SiO_2 particles: An elliptical assemblage of particles (ID: 1) with a 400 nm diameter was observed (Fig. 14-a). The primary components (Table 3) of the particles are O (62.8%) and Si (30.8%) with minor amounts of Fe (2.8%), Al (1.0%), K (0.6%) and Hg (2.1%). Several clear spots were recorded and shown in a pattern, suggesting crystalline oxide particles of Fe and Hg. The atomic percentages suggest that the particle is primarily SiO_2 with small amounts of Fe and Hg oxides.

TiO_2 particles: These particles often have a definite crystal habit with sizes ranging from 100 nm to 500 nm. A euhedral crystal particle (ID: 2) with a size of 200 nm was observed (Fig. 14-b). The primary components (Table 3) of the particle are O (39.4%) and Ti (58.7%), with a small amount of impurities. The SAED result indicated that it is a single crystal. The atomic ratio of O to Ti is close to 2 ($65.87/32.82 \approx 2$), suggesting that it is TiO_2 that contains minor amounts of impurities.

CaO particles: An irregular assemblage of Ca-bearing particles (ID: 3) (Fig. 15) is composed of O (27.2%) and Ca (72.1%), with minor amounts of Mg (0.5%) and Si (0.2%) (Table 3). Many diffraction spots were irregularly distributed, suggesting that the assemblage particles are polycrystalline. The atom percentages and the HRTEM image suggested that the particles are CaO with few impurities.

Iron oxide particles: A sub-circular assemblage of Fe-bearing particles (ID: 4) with a diameter of approximately 400 nm was observed (Fig. 16-a). The primary components of the particles (Table 3) are O (29.8%) and Fe (63.2%), with minor amounts of Mg (0.1%), Al (1.6%), Si (3.7%) and Ti (1.5%). The SAED result indicated that the particle is polycrystalline. The atom percentages and the SAED result suggested that the particles are Fe_2O_3 with some aluminum silicate.

(2) Sulfate particles: An irregular assemblage of Ca-bearing particles (ID: 5) was observed (Fig. 16-b). The size of the particle was approximately 1 μm. The primary components (Table 3) of the particles are O (45.1%), S (22.8%) and Ca (30.1%), with less than 1% Na, Al, Si and Fe. Based on the atomic ratio of O and S, this finding suggests that the particle may contain SO_4^{2-}. The SAED result revealed that the particle is a single crystal, indicating that the particles are $CaSO_4$.

A euhedral crystal particle (ID: 6) with a size of 100 nm × 200 nm was observed (Fig. 16-c). Its components (Table 3) are O (35.7%),

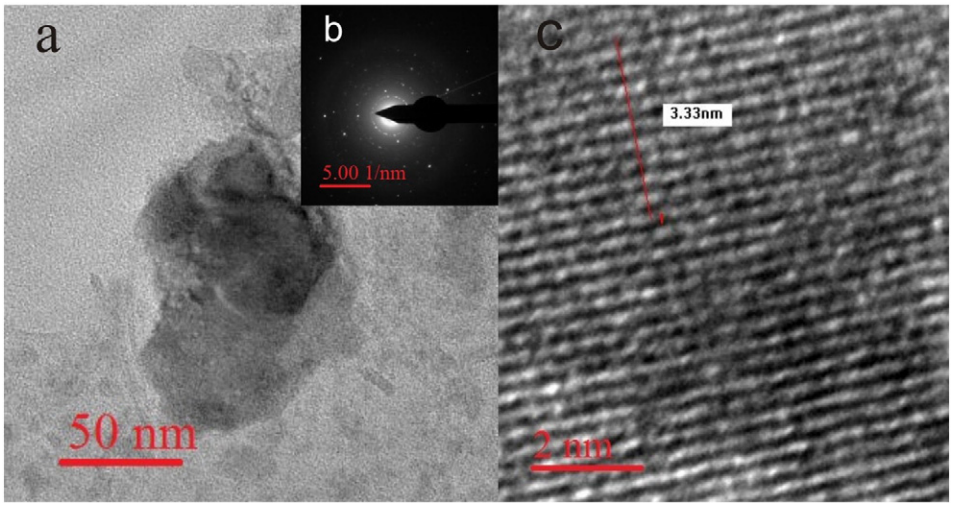

Fig. 9. Sb-bearing particles. (a) TEM image. (b) SAED pattern. (c) HRTEM image.

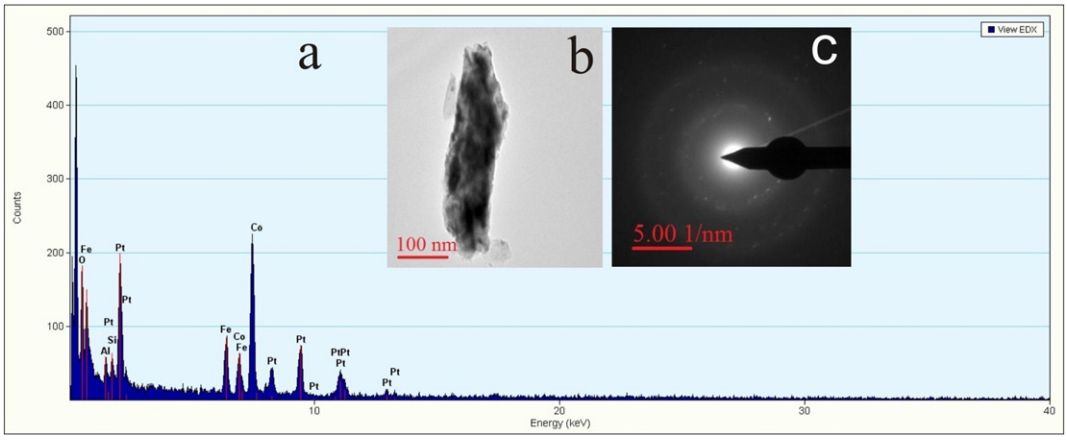

Fig. 10. Pt-bearing particles. (a) EDS results. (b) TEM image. (c) SAED pattern.

S (6.4%), Sr (19.8) and Ba (33.7%), with minor amounts of Na (0.1%), Al (0.6%), Ca (0.3%), Ti (2.8%), and Fe (0.6%). The atomic percentage and SAED result suggested that the particle is $BaSO_4$ that contains minor amounts of oxides.

(3) Aluminum silicate particles: A schistose particle (ID: 7) (Fig. 16-d) with a size of 200 nm × 300 nm is composed of O (67.4%), A (l5.3%), Si (16.3%), with minor amounts of Fe (1.0%) (Table 3). The SAED pattern suggests that it is made of crystalline oxide

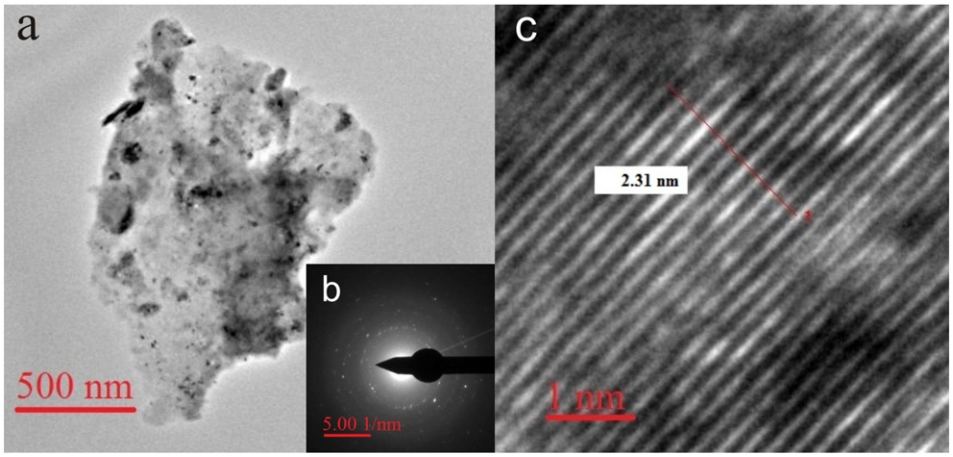

Fig. 11. Au-bearing particles. (a) TEM image. (b) SAED pattern. (c) HRTEM image.

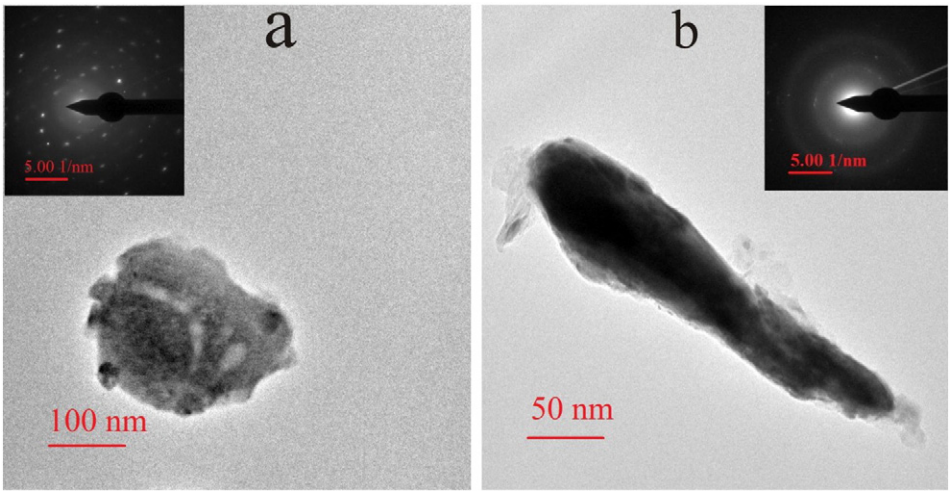

Fig. 12. TEM photomicrograph of (a) Y-bearing particles and (b) native V–Pt–Fe–Co alloy particles.

particles of Al and Si. Based on the atomic percentage and the morphology, it is suggested that the particle consists of Al_2O_3 and SiO_2.

5. Discussion and conclusions

5.1. Summary of the particles carried by the ascending gas flow: Characteristics and origins

The TEM observation indicated that there were metal sulfides and oxides/hydroxides (such as Fe_3O_4, Sb_3O_2, $Fe(OH)_3$ and PbS), native metal alloys (such as native vanadium–platinum–iron–cobalt alloy), nonmetallic oxides (such as SiO_2), chlorides (primarily NaCl), nonmetallic hydroxides (such as KOH) and sulfate (primarily $BaSO_4$) particles, as well as precious metal elements-(such as Au and Pt)bearing particles and rare earth elements-(such as Y)bearing particles in the ascending gas flow from the Dongshengmiao deposit.

The results of the 16 particles studied here indicated that the particles carried by the ascending gas flow were present in the form of single particles or aggregations with sizes ranging from 5 nm to 400 nm, which were sub-circular, circular, elliptical or irregular in shape. Most of the particles ranged from 100 nm to 200 nm in size, so that they were small enough to be adsorbed easily by micro-bubbles in the ascending gas flow. In addition, these particles have excellent absorptivity because of their high surface-to-volume ratio and because their surfaces are generally charged (Wei et al., 2013), so they could be carried and transported more easily by the ascending gas flow because of the mutual adsorption with micro-bubbles. These observations have been confirmed by the results of previous studies (Cao et al., 2009, 2010b; Etiope and Lombardi, 1996; Malmqvist et al., 1999; Tong et al., 1998; Wang et al., 1997; Wei et al., 2013; Xie et al., 1999; Zhou et al., 2003). The solid substances from the concealed ore bodies or other geological bodies can be carried and transported to the earth's surface by ascending gas flows from soil gas, atmosphere pumps, mineral weathering, organic decomposition and mantle degassing (Cameron et al., 2004; Etiope and Martinelli, 2002; Malmqvist and Kristiansson, 1984; Wang et al., 2007). Hence, the concealed ore bodies may be detected by capturing the ascending gas flow matter and analyzing them by using the modern analysis techniques. The components of the concealed ore bodies and rock wall can be deduced by analyzing the modality, shape, size, structure, composition and atomic ratio of the particles carried by the ascending gas flow.

With regards to the structure, most of the particles were crystalline, including single crystals and polycrystalline. Native vanadium–platinum–iron–cobalt alloys were first observed in the ascending gas flow at the Dongshengmiao deposit. Cao et al. (2009) first used TEM to identify the native gold particles in the ascending gas flow at the Changkeng concealed gold deposit, Guangdong Province, Southern China. Cao et al. (2010b) also used the TEM to discover the native copper, native copper–iron alloy, and native chromium–iron–copper alloy in the ascending gas flow at the Tongchanghe copper mine,

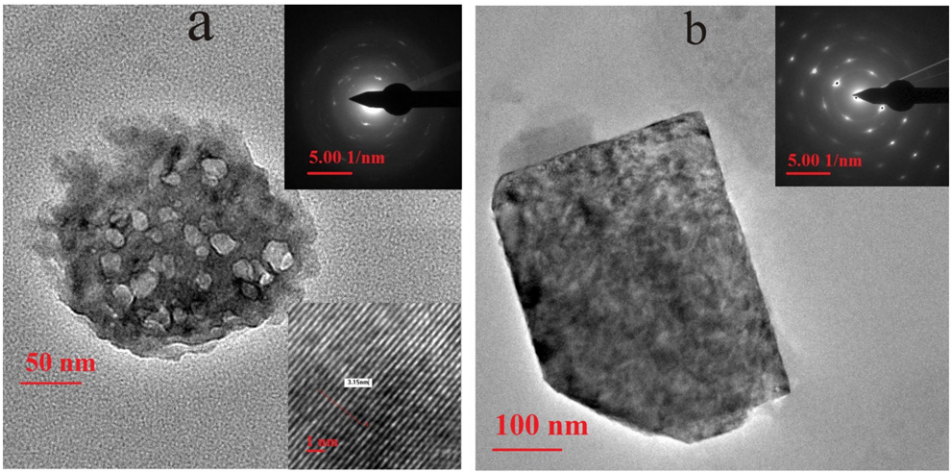

Fig. 13. TEM photomicrograph of (a) Ba-bearing particles and (b) an NaCl particle.

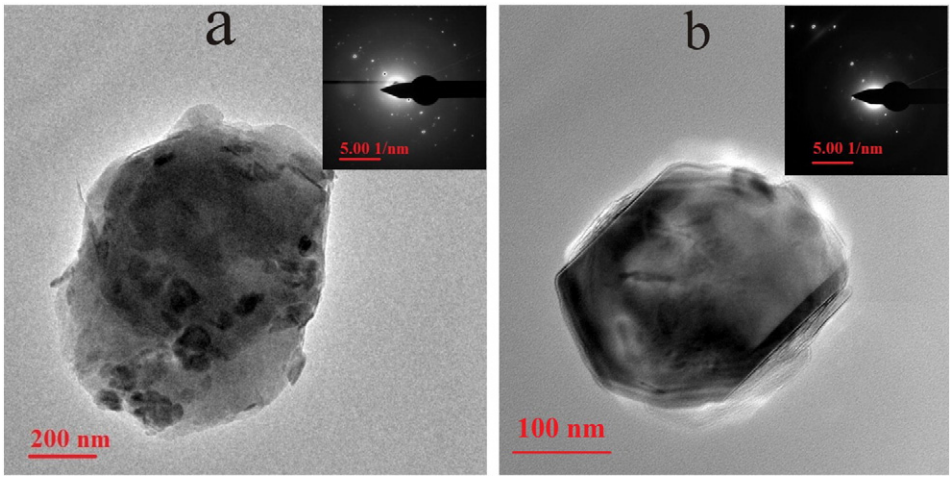

Fig. 14. TEM photomicrograph of (a) SiO_2 particles and (b) a TiO_2 particle.

Guizhou Province, China. These findings suggested that many types of native metal alloys can be transported by the ascending gas flow, and the transported forms of the particles in the ascending gas flow are varied.

In addition to some common elements (such as O, Si, Fe, Na, K, Ca, Mg, Al, Cl, P, and Ti) that were found in the particles carried by the ascending gas flow, metallogenic elements (such as S, Fe, Cu, Zn, and Pb) and their associated component elements (such as F, Co, As, and Au) were observed, which are closely related to ore minerals in concealed ore bodies. These results were consistent with previous studies (Peng and Zhai, 2004; Xia, 1992; Zhang et al., 2010). By analyzing the atomic percentages, the SAED patterns and the HRTEM image of the particles, we could characterize them as oxides, sulfides, carbonates, sulfates, chlorides, native metal alloy and possibly hydroxides. For instance, the primary composition of particle 1 is Fe_3O_4, which may have originated from magnetite. Particles 2 may contain some $Fe(OH)_3$ that most likely originated from siderite. The composition of siderite is $FeCO_3$, which is a soluble substance, and it can be soluble in $Fe(OH)_3$ at normal temperature, with the chemical equation $3CO_3^{2-} + 2Fe^{3+} + 3H_2O = 2Fe(OH)_3 + 3CO_2$. Particle 8 may contain some PbS that most likely originated from galena. The $BaSO_4$ particles most likely originated from barite, and the SiO_2 particles most likely originated from quartz. These results indicated that the particles carried by the ascending gas flow from the ore region could directly reflect information about the concealed ore bodies and wall rock, showing a good correlation with these regions. The ore minerals can be deduced by analyzing the particles carried by the ascending gas flow.

Table 3
EDS results for the soil particles (1–7).

Element	Particle number						
	1	2	3	4	5	6	7
Weight_O (%)	62.76	39.36	27.23	29.83	45.1	35.68	67.43
Atomic_O (%)	76.45	65.87	48.26	57.84	64.91	74.2	78.35
Weight_Na (%)					0.13	0.1	
Atomic_Na (%)					0.13	0.15	
Weight_Mg (%)			0.48	0.05			
Atomic_Mg (%)			0.56	0.06			
Weight_Al (%)	0.97	0.26		1.64	0.3	0.61	15.3
Atomic_Al (%)	0.7	0.26		1.89	0.25	0.76	10.54
Weight_Si (%)	30.78	0.49	0.16	3.72	0.93		16.27
Atomic_Si (%)	21.36	0.47	0.16	4.11	0.77		10.77
Weight_S (%)					22.82	6.38	
Atomic_S (%)					16.39	6.62	
Weight_Cl (%)		0.03					
Atomic_Cl (%)		0.02					
Weight_K (%)	0.61						
Atomic_K (%)	0.3						
Weight_Ca (%)			72.11		30.05	0.33	
Atomic_Ca (%)			51		17.26	0.27	
Weight_Ti (%)		58.71		1.49		2.76	
Atomic_Ti (%)		32.82		0.96		1.92	
Weight_Fe (%)	2.78	1.1		63.24	0.64	0.64	0.98
Atomic_Fe (%)	0.97	0.53		35.12	0.26	0.38	0.32
Weight_Sr (%)						19.76	
Atomic_Sr (%)						7.5	
Weight_Ba (%)						33.69	
Atomic_Ba (%)						8.16	
Weight_Hg (%)	2.06						
Atomic_Hg (%)	0.2						

In addition, the particles contained some elements that were not present in the previous studies but were abundant in our results (such as Mo, Sb, Pt and Y). Pt-bearing particles were first observed in the ascending gas flow, suggesting that Pt can be carried and transported in the nano-particles by the ascending gas flow, but it is not clear whether the particle is in the form of oxides or native matter. Moreover, Y-bearing and a number of Mo-bearing particles were observed.

The particles carried by the ascending gas flow could not only to be used to deduce the ore minerals in the concealed ore bodies, but they could also reflect the types of mineral assemblages in the ore bodies. In our studies, the element associations of the particles carried by the ascending gas flow were often observed as S–Fe–Zn, S–Fe–Pb–Zn, S–Cu, S–Zn, S–Pb, S–Pb–Zn, S–Fe–Cu or S–Fe–Cu–Mo, and Cr–Mn–Fe. These results are consistent with those of the previous studies. The Donghshengmiao deposits were rich in poly-metal (such as Fe, Cu, Zn and Pb) sulfide. Metallogenic elements were found as S–Cu, S–Cu–Zn, and S–Fe–Pb–Zn forms in the vertical profile and S–Cu–Pb, S–Pb–Zn, S–Zn, and S–Fe in the horizontal direction. The ore mineral assemblages were primarily pyrite–pyrrhotite (S–Fe), pyrite–pyrrhotite–chalcopyrite (S–Fe–Cu), pyrite–sphalerite (S–Fe–Zn), galena–sphalerite (S–Zn–Pb), pyrite–chalcopyrite and galena–sphalerite–pyrrhotite–pyrite (S–Fe–Zn–Pb) (Table 4) (Peng and Zhai, 2004; Xia, 1992; Zhang et al., 2010). The polycrystalline S–Fe–Zn particles were sub-circular or elliptical, with sizes ranging from 50 nm to 200 nm (Table 4). The Fe and Zn contents of these particles were negatively correlated, and overall, their Fe content is higher than their Zn content. In a study by (Xia, 1992), Fe and Zn were negatively correlated, with a correlation coefficient of −0.6495, and Fe was usually substituted isomorphically for Zn in sphalerite. Our result also supports this observation. The S–Fe–Zn particles may have originated from the mineral assemblages of pyrite–sphalerite.

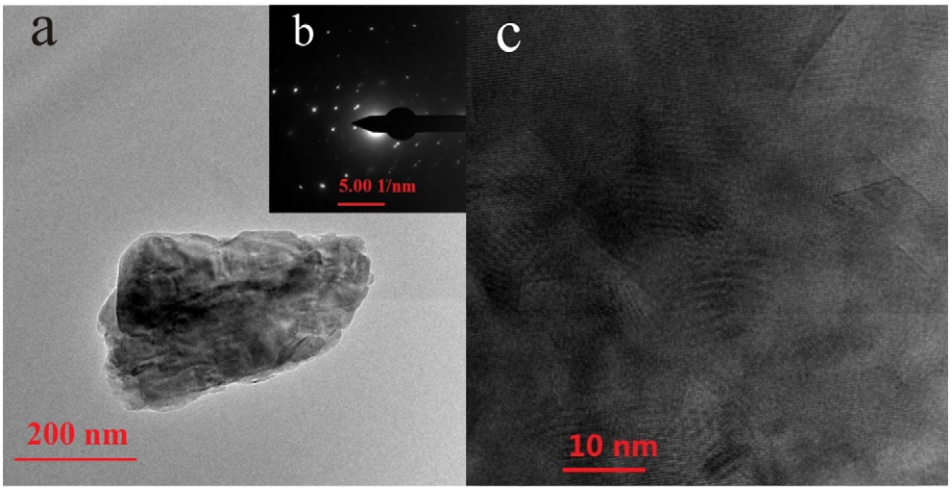

Fig. 15. CaO particles. (a) TEM image. (b) SAED pattern. (c) HRTEM image.

The S–Fe–Cu particles were polycrystalline with sub-circular, elliptical or irregular shapes, and they ranged in size from 50 nm to 400 nm (Table 4). The Fe and Cu element contents were negatively correlated. The S–Fe–Cu particles may have originated from the mineral assemblages of the pyrrhotite–pyrite–chalcopyrite. The S–Pb–Zn particles were polycrystalline, with the shape of circular or sub-circular, and ranged in size from 100 nm to 200 nm (Table 4). The contents of Zn and Pb element were negatively correlated. The S–Pb–Zn particles may have originated from the mineral assemblages of galena–sphalerite. The Cr–Mn–Fe particles were sub-circular, elongated or irregular in shape, with sizes ranging from 50 nm to 400 nm (Table 4). The Cr, Mn and Fe contents were positively correlated, the Fe content (usually ranging from 40% to 70%) were the highest and the Mn content were the lowest. Some Cr–Mn–Fe bearing particles contained Cu or Zn. There were a large number of Cr–Mn–Fe bearing particles, but it is not clear whether the Cr–Mn–Fe bearing particles

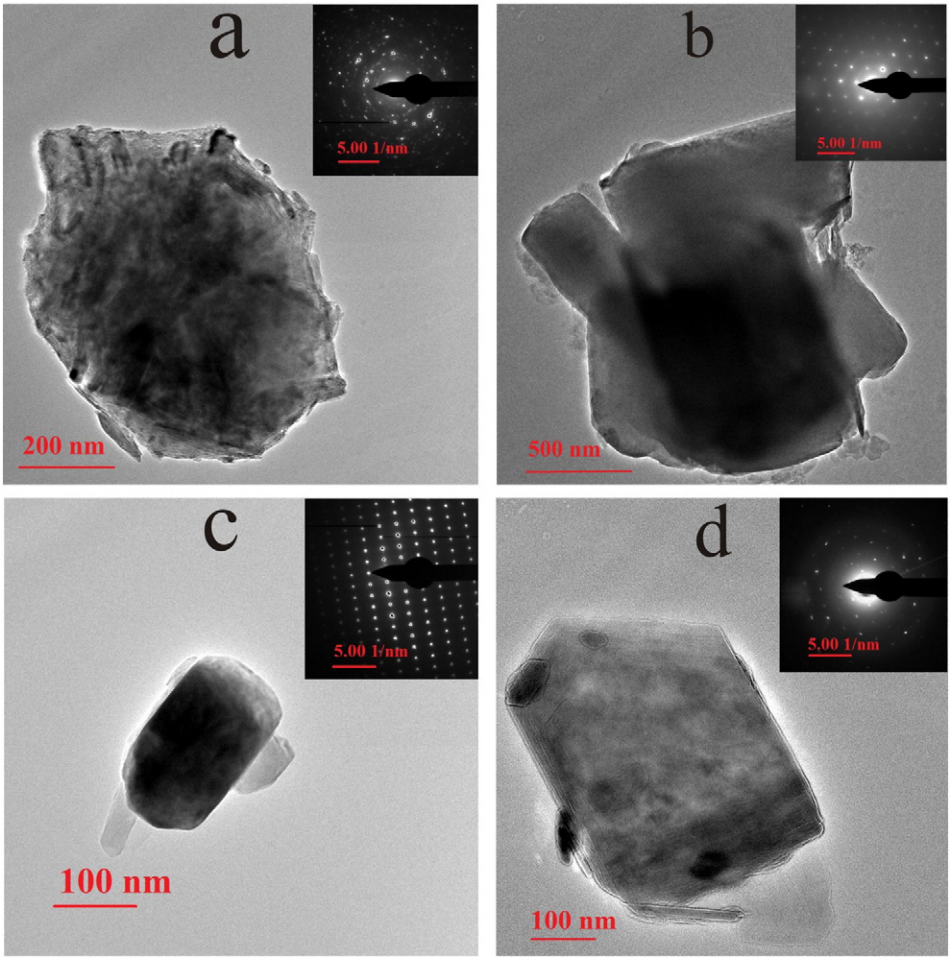

Fig. 16. TEM photomicrograph of (a) Fe-bearing particles, (b) Ca-bearing particles, (c) a $BaSO_4$ particle and (d) a Al and Si-bearing particle.

Table 4
Ore body types, ore mineral assemblages, and the particles carried by the ascending gas flow: Characteristics of the 14th exploration line from the Dongshengmiao deposit.

Previous studies of ore bodies[a]		Particles carried by the ascending gas flow in our samples		Sampling points
Types	Mineral assemblages	Element association	Characteristics	
Zinc-sulfide ore body	Gn + Sph/Pyr + Py + Sph/ Pyr + Sph/Py + Sph/ (Py) + Pyr + Gn + Sph/ /Cp + Py + Sph/ Cp + Gn + Py + Pyr + Sph/ Sph + Py/Sph + Pyr/ Sph + Pyr + Py	S–Pb–Zn/S–Pb/S–Zn/S–Fe–Zn	Sub-circular, elliptical or irregular/50 nm to 400 nm/polycrystalline	Nos: 1–43
Single-sulfide ore body	Py/Pyr + Py/(Sph) + Pyr/ (Sph) + Pyr + Py/ (Sph) + Py	S–Fe/S–Fe–Zn/S–Pb	Sub-circular or elliptical/50 nm to 200 nm/polycrystalline	Nos: 1–43
Copper-sulfide ore body	Gn + Sph + Pyr + Cp Gn + Sph + Py + Cp Cp + Gn + Sph + Pyr + Py	S–Fe–Cu/S–Fe–Cu–Mo/S–Cu/O–S–Cu	Sub-circular, elliptical or irregular/50 nm to 400 nm/polycrystalline	Nos: 23–43
Siderite ore body	Sid/Pyr + Sid/ (Mt) + Py + Pyr + Sid/ (Mt) + Sid	S–Fe/Cr–Mn–Fe	Sub-circular, elongated or irregular/50 nm to 400 nm/polycrystalline	No independent ore body in this exploration profile

PS: Cp — chalcopyrite; Sid — siderite; Gn — galena; Mt — magnetite; Py — pyrite; Pyr — pyrrhotite; Sph — sphalerite.
[a] The data for the ore bodies types and ore mineral assemblages of this deposit are from Peng and Zhai (2004) and Zhang et al. (2010).

were oxides or a native alloy. These results indicated that the mineral assemblages of a deposit can be deduced by analyzing the elemental association of the particles carried by the ascending gas flow.

5.2. Comparison of particles carried by the ascending gas flow with soil particles

Previous studies on geogas prospecting indicate that the substance from the concealed ore bodies or other geological bodies can be carried and transported to the earth's surface by the ascending gas flow, which might be in the form of micro-bubbles that are formed not only via diffusion and groundwater, but also via vertical movement or Brownian motion. The origins and migration forms of the particles carried by the ascending gas flow are one of the important problems to solve in geogas prospecting, and they play an extremely important role in the application of deposit prospecting (Cao, 2011; Cao et al., 2009, 2010a; Etiope and Lombardi, 1996; Kristiansson and Malmqvist, 1980, 1982; Zhou et al., 2003). In our studies, the particles carried by the ascending gas flow and the corresponding soil samples were collected and analyzed by TEM technique. The analysis results indicated that the particles carried by the ascending gas flow showed a good correlation with the known ore bodies. However, the soil particles showed apparent differences with the particles carried by the ascending gas flow.

In appearance, the soil particles were lighter, and their sizes commonly ranged from 200 nm to 500 nm and over 500 nm. These particles usually had clear and sharp edges, with a regular shape. The particles carried by the ascending gas flow were darker because they contained heavy metal elements, and their sizes often ranged from 100 nm to 200 nm with a sub-circular or elliptical shape. In short, the particles carried by the ascending gas flow were much smaller than the soil particles. For some typical examples, the SiO_2 from the soil particles (Fig. 17-b) had a regular shape and sharp edges, and the particles carried by the ascending gas flow were circular in shape (Fig. 17-a). The soil particles (Fig. 17-d) containing Fe also exhibited sharp edges with a size of 400 nm × 500 nm, and the particles carried by the ascending gas flow (Fig. 17-c) containing Fe were sub-circular with a 100 nm diameter. These features indicated that the formation mechanism and migration forms of the soil particles and the particles carried by the ascending gas flow are different. This morphological contrast indicated that the particles carried by the ascending gas flow have traveled a long migrational distance.

In terms of composition, the soil particle samples were primarily nonmetallic oxide, sulfate and aluminum silicate, and a large amount of metal sulfides and oxides/hydroxides (such as Fe_3O_4, Sb_3O_2, $Fe(OH)_3$ and PbS), native metal alloy, precious metal element and rare earth element-bearing particles showing a good correspondence to the concealed ore bodies were found in the particles carried by the ascending gas flow. The soil particle samples that contained common elements (such as O, Na, Mg, Al, Si, Ca, and Ti) are closely related to the earth's surface and had a high oxygen content, which indicated that the formation conditions of the soil particles were close to the surface oxidation environment. Heavy metal element-(such as As, Hg, and Zn)bearing particles were found in the soil particles, suggesting that some metallogenic element bearing particles from the concealed ore body may be absorbed by soils such as clays, colloids and salts, when the particles were transported upward to the surface (Wang et al., 2012; Ye et al., 2014).

For instance, the components of the soil particles at the No. 4 sampling point are O (33.2%), Mg (23.0%) and Ca (38.7%), with a small amount of Al (0.7%), Si(1.4%), and Fe (1.6%), and the corresponding particles carried by the ascending gas flow are composed of O (53.6%), F (1.7%), Mg (0.1%), Al (1.0%), Si (3.3%), P (0.8%), S (6.3%), Cl (0.4%), Ca (2.0%), Fe (2.5%), Cu (5.7%) and Mo (22.5%). The particles that were carried by the ascending gas flow contain the elements that are closely related to the concealed ore bodies (such as S, Cu and Mo). The components of the soil particles at the No. 10 sampling point are O (57.3%), Si (21.6%) and K (12.0%), with minor amounts of Mg (0.6%), Al (7.2%) and Fe (1.3%), and the corresponding particles carried by the ascending gas flow are composed of O (52.2%), Na (7.4%), Mg (1.4%), Al (2.3%), Si (19.2%), S (0.7%), K (3.4%), Ca (5.6%), Fe (0.9%), Co (0.2%), Zn (5.4%) and Pb (1.4%). Similar to the No. 4 sampling point, the particles carried by ascending gas flow contain S, Zn and Pb, which are the metallogenic elements of the concealed ore bodies.

These results further demonstrated that the particles carried by the ascending gas flow and the soil particles originated directly from the deep concealed ore bodies. In addition, some metallogenic element-bearing particles were found in soil and geogas samples, suggesting that metal particles from the ore body can be carried and transported by the ascending gas flow to the earth's surface, arriving at the surface; part of the particles persist in the ascending gas flow and the other part of the particles are trapped by soil geochemical barriers (Wang et al., 2012; Ye et al., 2014).

5.3. Comparison of particles carried by the ascending gas flow from the Dongshengmiao deposit with those from other deposits

The properties of the overlying layer and the buried depth of ore bodies from the four deposits are different (Table 5). By comparing our work with the investigation of particles carried by the ascending gas flows from the Fankou Lead–Zinc deposit (Wei et al., 2013), the

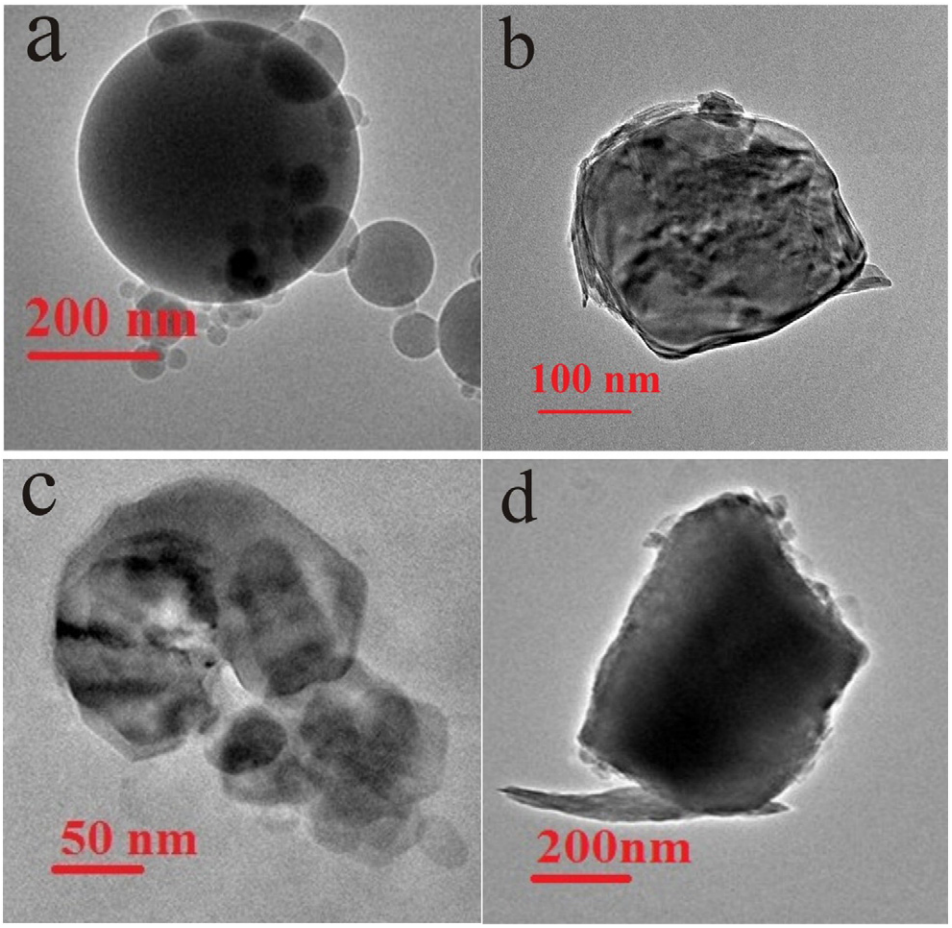

Fig. 17. Comparison of particles carried by the ascending gas flow and the soil particles. (a) SiO_2 particles carried by the ascending gas flow. (b) SiO_2 from soil particles. (c) Fe-bearing particles carried by the ascending gas flow. (d) Fe-bearing particles from soil particles.

Tongchanghe Copper deposit (Cao et al., 2010b) and the Changkeng Gold deposit (Cao et al., 2009), we can conclude the following differences (Table 5). With respect to the appearance, the particles from the four deposits mostly ranged in size from 100 nm to 200 nm, i.e., less than 500 nm. However, particles from Dongshengmiao polymetallic pyrite deposit are primarily circular, sub-circular or elliptical in shape, and the particles from the Fankou Lead–Zinc deposit are mostly regular (such as plate-shaped, trigonal and spherical) with clear edges. The shapes of the particles from the Tongchanghe copper deposit are similar to those of the Dongshengmiao deposit, i.e., primarily sub-circular and elliptical, but the particles from the Changkeng gold deposit are irregularly globular.

As to the composition, the particles carried by the ascending gas flow of the Fankou Lead–Zinc deposit are primary Cu-bearing, Zn-bearing and Pb-bearing particles; the particles in the Tongchanghe Copper deposit are primary Cu-bearing particles, native copper and native chromium–iron–copper alloy; the Changkeng Gold deposit have Au-bearing, Hg-bearing and W-bearing particles; and the Dongshengmiao polymetallic pyrite deposit primary have mainly Fe-bearing, Cu-bearing, Zn-bearing, Pb-bearing, Mo-bearing and even Au-bearing, Pt-bearing, and Y-bearing particles. These results indicated that different particles carried by the ascending gas flow are from different types of deposits, and they are closely related to ore minerals in concealed ore bodies. The particles carried by the ascending gas flow could reflect the metallogenic information about the deep concealed ore body directly, without interference from the properties and thickness of the overlying layer. In other words, geogas prospecting could be used to explore different types of ore deposits.

5.4. Spatial relation between the particles carried by the ascending gas flow and the concealed ore bodies

We analyzed the weights of the particles containing Cu–Zn–Pb after the homogenization of each sampling point along the 14th exploration line (Fig. 18). Zn-bearing and Cu-bearing particles were commonly observed in the ore region, and there was a high Cu-bearing particle content (the Cu content of the particle from the No. 1 sampling point was up to 82.5%), and Pb-bearing particles were only found in part of this position. These results suggested that the particles carried by the ascending gas flow from the 14th exploration line of the ore region showed a good spatial correlation with the known concealed ore bodies. The exploration profile (Fig. 19) shows that the 14th exploration line is primarily zinc sulfide-rich ore body, zinc sulfide ore body, single zinc ore body, copper sulfide ore body and single sulfide, but it does not form a continuous lead ore body. The zinc ore bodies were more widely distributed than the copper or lead ore bodies. To better analyze the spatial relations between the particles and concealed ore body, we divided the exploration line into four segments for analysis according to the sampling number.

The particles from the Nos. 1–10 sampling points primarily contained Fe, Zn, Pb and Cu (Fig. 20). Fe-bearing particles were observed at all the sampling points, and the Zn, Pb and Cu-bearing particles occurred 6, 3 and 2 times, respectively. Most of the Fe-bearing particles were over 40.0 wt.%, and the No. 8 sampling point exhibited a value of 65.8%. Pb-bearing particles were 42.9% at the No. 5 sampling point and Cu-bearing particles were up to 82.5% at the No. 1 sampling point, and the Zn-bearing particles had small amounts of

Table 5
A comparison of the particles carried by the ascending gas flows from four different deposits (Cao et al., 2009, 2010a, b; Wei et al., 2013).

Deposits			Major ore minerals/Gangue minerals	Particles carried by the ascending gas flow		
Name	Ore genesis/buried depth	Exposed strata/rock types		Type/size/shape		
① Dongshengmiao polymetallic pyrite deposit (Inner Mongolia Province, China)	A sedimentary exhalative (SEDEX) deposit/400 m to 1000 m	Middle Proterozoic Langshan Group, Mesozoic Lisangou formation, Tertiary, and Quaternary/quartzite, two-mica quartz schist, sericite quartz schist, quartz conglomerate, dolomitic-marble, schist, graphite sericite schist, carbon phyllite, conglomerate and sandstone	Pyrite, pyrrhotite, sphalerite, siderite, galena, chalcopyrite, marcasite and magnetite/dolomite, calcite, quartz, mica and graphite	① Native alloy (V–Pt–Fe–Co) ② Sulfides (PbS) ③ Oxides (Fe_3O_4, Sb_3O_2, SiO_2, Cu, Zn, Mo oxides) ④ Chlorides (NaCl) ⑤ Hydroxides ($Fe(OH)_3$ and KOH) ⑥ Sulfate ($BaSO_4$) ⑦ Other particles: Au-bearing, Pt-bearing, Y-bearing	5 nm to 400 nm (mostly 100 nm to 200 nm)	Mostly circular, subcircular, elliptical
② Fankou lead–zinc deposit (Guangdong Province, China)	A submarine hydrothermal spring effusion type Pb–Zn deposit/100 m to 700 m	Cambrian, Devonian, Carboniferous, Permian rocks and Quaternary/terrigenous, pyrite shale, fossils, carbon, clay minerals, carbonate rock containing clay and carbonate rock	Pyrite, sphalerite, galena, chalcopyrite, arsenopyrite and stibnite/Calcite, dolomite, quartz, Siderite, chlorite, barite and dolomite	① Oxides (SiO_2, TiO_2, Pb–Mo oxides) ② Sulfides (PbS and ZnS) ③ Chlorides (KCl) ④ Sulfates ① Silicates ⑥ Hydroxides	10 nm to 300 nm (mostly 100 nm to 200 nm)	Mostly regular (plate-shape), trigonal, spherical
③ Tongchanghe Copper deposit (Guizhou Province, China)	A basalt type copper deposit formed by syn-volcanic hydrothermal mineralization superimposed by buried metamorphic transformation/20 m to 300 m	Lower Permian Maokou Formation, Upper Permian Emeishan Basalt and Xuanwei Formation and Quaternary sediments/compact massive basalt, amygdaloidal and esite-basalt, olivine basalt, volcanic agglomerate, volcanic breccia, tuff breccia, tuff and sedimentary tuff	Chalcocite, bornite, malachite, azurite, covellite, chalcocite, cuprite, natural copper/Pyroxene, chlorite, quartz, chalcedony, calcite, dolomite, laumontite, carbon asphalt and gypsum	① Native metal or alloy (native cooper, native Cu–Fe alloy, native Cr–Fe–Cu alloy) ② Chlorides (KCl) ③ Oxides (SiO_2, TiO_2, Al_2O_3, CuO) ④ Sulfates ($CaSO_4$) ⑤ Hydroxides ($Cu(OH)_2$ and $Fe(OH)_3$)	5 nm to 500 nm (mostly 50 nm to 200 nm)	Mostly subcircular, elliptical,
④ Changkeng Gold deposit (Guangdong Province, China)	A large Carlin disseminated type gold deposit/50 m to 100 m	Lower Carboniferous, Upper Triassic rocks and Quaternary sediments/Limestone, silty shale, sandstone, siltstone, arkosic quartz sandstone, siltstone, bioclastic limestone, muddy limestone, and carbonaceous mudstone	Pyrite, realgar, orpiment, antimonite, marcasite, cinnabar, arsenopyrite, and sphalerite/quartz, calcite, barite, illite, dickite, fluorite, and gypsum	① Native metal (native gold) ② Oxides (Fe_2O_3, WO_3, TiO_2) ③ Sulfates ($PbSO_4$) ④Hg-bearing	10 nm to 300 nm (mostly 100 nm to 200 nm)	Mostly irregular globular

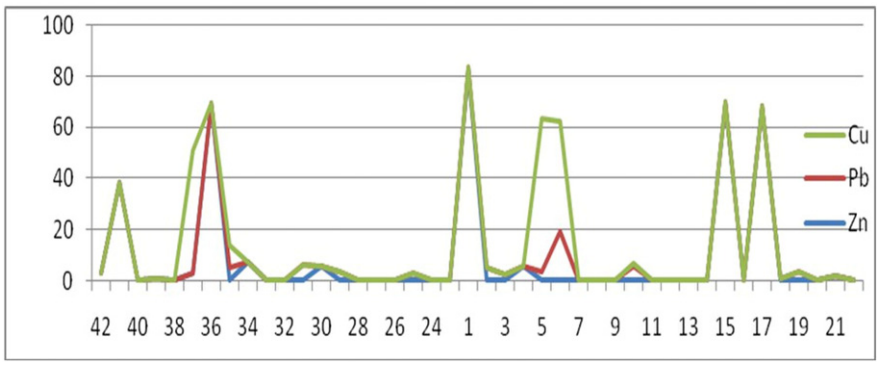

Fig. 18. The homogenization of the Cu–Zn–Pb weight percentage of each sampling point along the 14th exploration line from the Dongshengmiao polymetallic pyrite deposit.

weight percentages. These data indicate that Fe usually substituted isomorphically for Zn in the sphalerite from this deposit, which has been confirmed by Xia (1992). Most of the particles were in the form of oxide or sulfide. The analysis indicated that there are strong elemental anomalies in terms of Fe, Zn, Pb and Cu in the area. These results are consistent with the results of the exploration profile research. The Nos. 1–10 sampling points are above the single sulfide ore bodies, zinc sulfide ore bodies and copper sulfide ore bodies.

The particles primarily containing Fe, Zn, Cu and Pt elements were observed at the Nos. 11–22 sampling points (Fig. 21). Fe-bearing particles were observed in most of the sampling points, except for the No. 16 sampling point. The Zn, Cu and Pt-bearing particles occurred 5, 3 and 2 times, respectively. Most of the Fe-bearing particles were over 40.0 wt.%. Cu-bearing particles were up to 69.6% at the No. 15 sampling point and Pt-bearing particles was up to 59.6% at the No. 4 sampling point, and the Zn-bearing particles made up minor amounts of the content. The particles were in the form of native alloy, S–Fe–Zn, S–Fe–Cu and oxides. In addition, the Y element was present at the No. 17 sampling point, at a weight percentage of 40.0%. The analysis indicated that the mineralization elements of Cu and Zn were anomalies in this sampling area. These results are consistent with the known research. The exploration profile studies indicated that the Nos. 11–22 points are spread over the single sulfide ore body and the zinc sulfide ore body. In addition, there are faults under the sampling points. These results suggest that the fault provides a good channel for the ascending gas flow, and when there is a fault or fracture, the particles carried by the ascending gas flow will primarily migrate along them.

The particles containing Fe, Zn, Mo and Cu were observed at the Nos. 23–32 sampling points (Fig. 22). Fe-bearing particles were observed at all the sampling points, and the Zn, Mo and Cu-bearing particles occurred 4, 3 and 1 times, respectively. Most of the weight percentages of the Fe-bearing particles were over 50.0%, and Mo-bearing particles were up to 52.7% at the No. 29 sampling point. In addition, Au-bearing particles were observed at the No. 27 sampling point, with a weight percentage of 35.7%. The Nos. 23–32 sampling points overlay a thick ore body that is buried deeper, which contains large rich, zinc sulfide ore body, zinc sulfide ore body, copper sulfide ore body and single-sulfide ore body. The discovery of the Fe, Zn, Cu and Mo-bearing particles presents a powerful tool for the exploration of deep-seated concealed ore bodies.

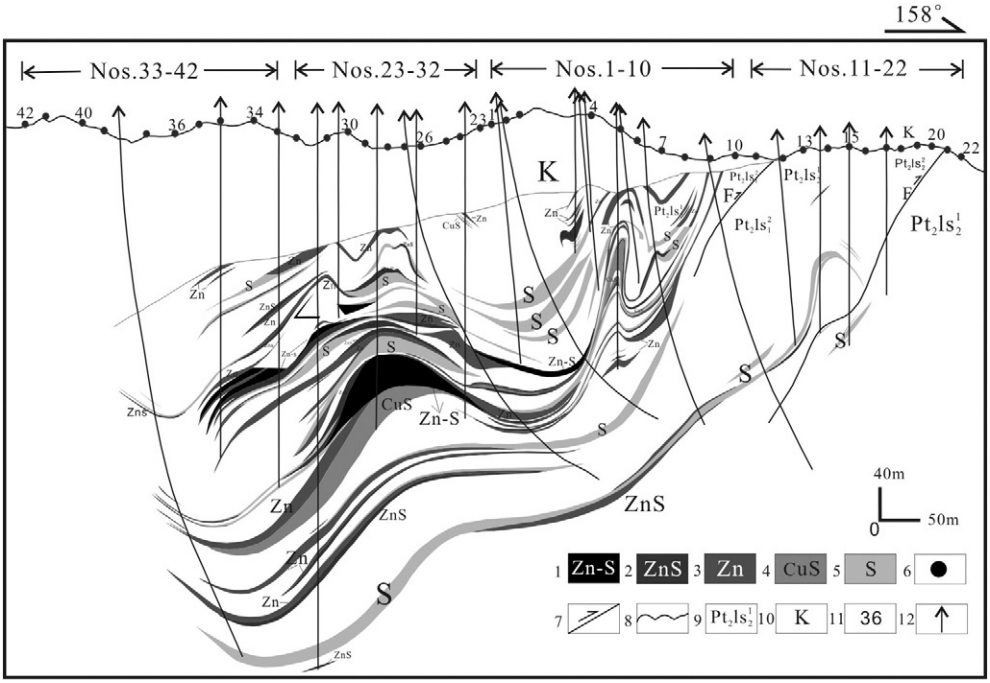

Fig. 19. A 14th prospecting line profile map of the Dongshengmiao polymetallic pyrite deposit (redrawn according to a profile map provided by Dongshengmiao Mineral Company Limited). 1 — rich-zinc sulfide ore body, 2 — zinc sulfide ore body, 3 — single zinc ore body, 4 — copper sulfide ore body, 5 — single sulfide ore body, 6 — sampling point, 7 — fault, 8 — stratigraphic boundary, 9 — the member of the Mesoproterozoic Langshan group, 10 — Cretaceous, 11 — sampling number, and 12 — drilling.

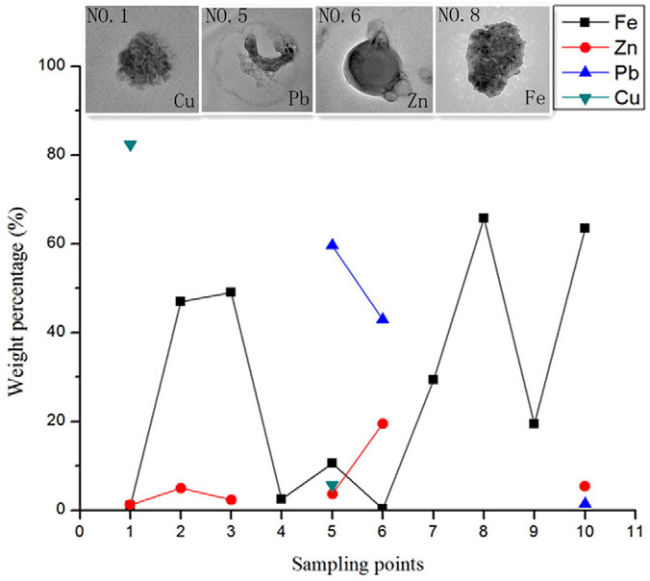

Fig. 20. Fe–Zn–Pb–Cu elemental distribution of the Nos. 1–10 sampling points.

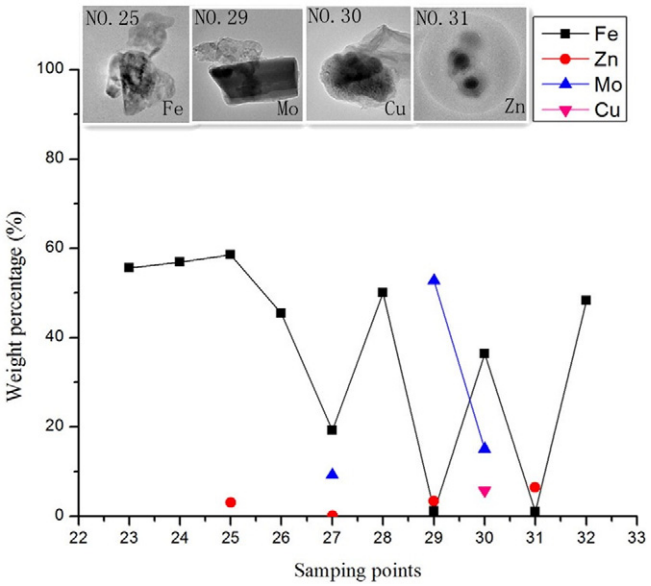

Fig. 22. Fe–Zn–Mo–Cu elemental distribution of the Nos. 23–32 sampling points.

The particles containing Fe, Cu, Pb and Mo were observed at the Nos. 33–42 sampling points (Fig. 23). Fe-bearing particles were present at all the sampling points. The Cu, Mo and Pb-bearing particles occurred 6, 4 and 2 times, respectively. Most of the Fe-bearing particles were over 70.0 wt.%, and they were up to 80.2% at the No. 36 sampling point. The particles were in S–Fe–Cu, S–Fe–Cu–Mo, S–Fe–Mo, Cr–Mn–Fe or oxides forms. The Nos. 33–42 sampling points overlay the single zinc ore body, the zinc sulfide ore body, the rich zinc sulfide ore body and the copper sulfide ore body. This sampling area is located in the northern part of the ore body, at the edge of the primary ore body. The results show that the Fe, Cu, Pb and Mo-bearing particles were observed widely and exhibited the highest average value for weight percentages. The observation of the particles containing Fe, Cu, Pb and Mo suggests that these particles are significant for exploring the concealed ore body in this area.

According to the above analysis, the comparison of the particles carried by the ascending gas flow from each sampling point with the concealed ore bodies shows a good spatial correlation with the known concealed ore bodies (Table 4). A large number of particles containing the metallogenic elements Fe, Zn, Cu and Pb were found, and an EDS, SAED pattern or HRTEM image was used to analyze the composition and the crystal structure, suggesting that they may have originated from pyrite, pyrrhotite, sphalerite, galena, chalcopyrite, siderite and magnetite, which are the primary ore minerals of the concealed ore bodies. These results indicated that the types of concealed ore bodies can be deduced by analyzing the particles carried by the ascending gas flow.

Geogas prospecting is a relatively new technique for exploring deep-seated and concealed deposits, and it has advantages relative to the traditional geochemical techniques because the particles carried by ascending gas flows are a direct part of the concealed deposit instead of coming from secondary source data, and they can be located hundreds of meters deep or the geological bodies can even be located thousands of meters deep, without interference from the properties and thickness of the overlying layer. Not only the composition of mineral and wall rock

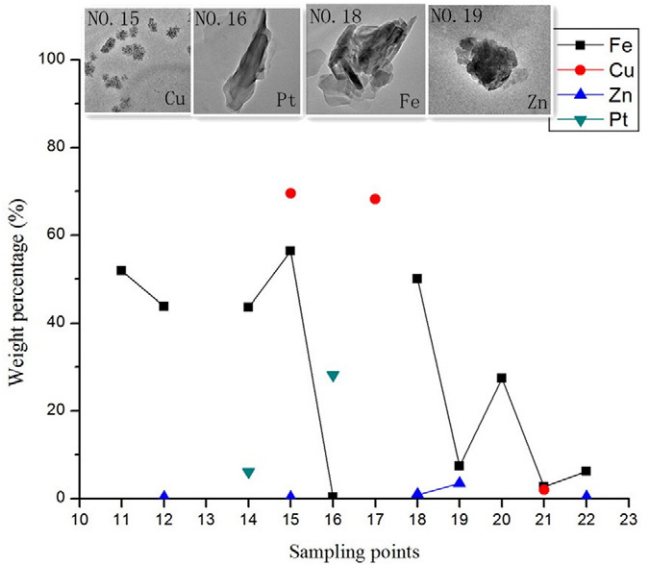

Fig. 21. Fe–Zn–Cu–Pt elemental distribution of the Nos. 11–22 sampling points (the sample from the No. 13 sampling point was invalid).

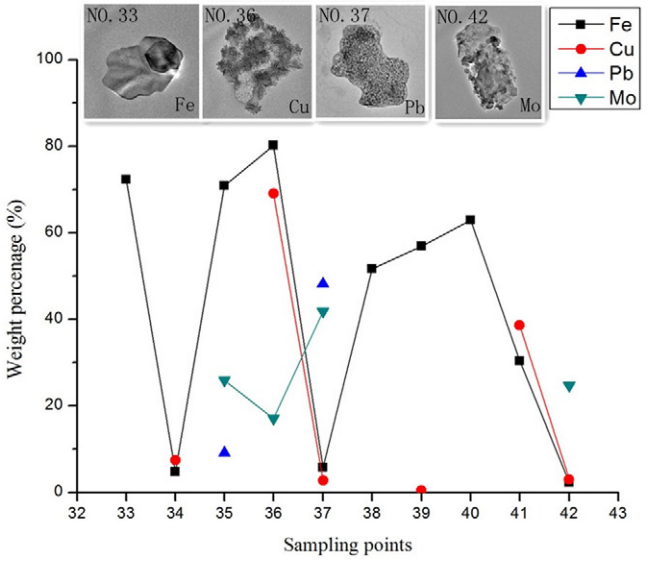

Fig. 23. Fe–Cu–Pb–Mo elemental distribution of the Nos. 33–42 sampling points.

but also the combination of ore mineral assemblages and even the types of ore bodies can be deduced by studying the morphology, composition and structure of particles carried by an ascending gas flow. However, this approach cannot be used to predict the scale or the range of a deposit, and it may be used in combination with other methods for further research.

Acknowledgments

This project was supported by the National Natural Science Foundation of China (grant nos. 41030425, 41072263, 40773037 and 40673044). The authors wish to thank Jian Yurong and Gao Wenge of the Dongshengmiao Mining Co., Ltd for the help in the sampling work and Huang QinLi and Liu Hongfei of the Instrument Analysis Center at Yangzhou University for the assistance with the TEM analysis.

References

Annunziatellis, A., Ciotoli, G., Lombardia, S., Nolasco, F., 2003. Short- and long-term gas hazard: the release of toxic gases in the Alban Hills volcanic area (central Italy). J. Geochem. Explor. 77, 93–108.

Cameron, E.M., Hamilton, S.M., Leybouren, M.I., Hall, G.E.M., Mccelenaghan, M.B., 2004. Finding deeply buried deposits using geochemistry. Geochem. Explor. Environ. Anal. 4, 7–32.

Cao, J.J., 2009. A technique for detecting concealed deposits by combining geogas particle characteristics with element concentrations. Met. Miner. 392 (2), 1–4 (in Chinese with English abstract).

Cao, J.J., 2011. Migration mechanisms of gold nanoparticles explored in geogas of the Hetai ore district, southern China. Geochem. J. 45 (3), e9–e13.

Cao, J.J., Hu, R.Z., Liu, S., 2005. Simulation test on migration of geogas-carrying gold nanoparticles in slope sediments. Miner. Depos. Res. Meet. Glob. Chall. 9, 897–900.

Cao, J.J., Hu, R.Z., Liang, Z.R., Peng, Z.L., 2009. TEM observation of geogas-carried particles from the Changkeng concealed gold deposit, Guangdong Province, South China. J. Geochem. Explor. 101, 247–253.

Cao, J.J., Liu, C., Xiong, Z.H., 2010a. Particles carried by ascending gas flow at the Tongchanghe copper mine, Guizhou Province, China. Sci. China Earth Sci. (Sci. China Ser. D) 53 (11), 1647–1654.

Cao, J.J., Hu, X.Y., Jiang, Z.T., Li, H.W., Zou, X.Z., 2010b. Simulation of adsorption of gold nanoparticles carried by gas ascending from the Earth's interior in alluvial cover of the middle-lower reaches of the Yangtze River. Geofluids 10 (3), 438–446.

Chiodini, G., Frondini, F., Ponziani, F., 1995. Deep structures and carbon dioxide degassing in central Italy. Geothermics 24, 81–94.

Etiope, G., 1998. Transport of radioactive and toxic matter by gas microbubbles in the ground. J. Environ. Radioact. 40, 11–13.

Etiope, G., Lombardi, S., 1996. Laboratory simulation of geogas microbubble flow. Environ. Geol. 27, 226–232.

Etiope, G., Martinelli, G., 2002. Migration of carrier and trace gases in the geosphere: an overview. Phys. Earth Planet. Inter. 129, 185–204.

Gold, T., Soter, S., 1980. The deep earth-gas hypothesis. Sci. Am. 242, 132–138.

Kristiansson, K., Malmqvist, L., 1980. A new model mechanism for the transportation of radon through the ground. Society of Exploration Geophysicists Fiftieth Annual International Meeting, Houston, Texas, pp. 2535–2565.

Kristiansson, K., Malmqvist, L., 1982. Evidence for nondiffusive transport of Rn in the ground and a new physical model for the transport. Geophysics 47, 1444–1452.

Kristiansson, K., Malmqvist, L., 1987. Trace elements in the geogas and their relation to bedrock composition. Geoexploration 24, 517–534.

Kristiansson, K., Malmqvist, L., Persson, W., 1990. Geogas prospecting: a new tool in the search for concealed mineralizations. Endeavor (New Series) 14, 28–33.

Ma, W.Y., Hui, Q., Xue, M., Ji, W.X., Chen, D.Y., 1997. Determination of the gold content in geogas by resonance ionization mass spectrometry. J. Anal. At. Spectrom. 12, 57–59.

Ma, W.Y., Xue, M., Zhang, J., Chen, D.Y., 1998. Ultrasensitive determination of gold in geogas by laser excited atomic fluorescence spectrometry. Spectrochim. Acta B 53, 1421–1425.

Malmqvist, L., Kristiansson, K., 1981. Microflow of geogas — a possible formation mechanism for deep-sea nodules. Mar. Geol. 40, M1–M8.

Malmqvist, L., Kristiansson, K., 1984. Experiment evidence for an ascending micro-flow of geogas in the ground. Earth Planet. Sci. Lett. 70, 407–416.

Malmqvist, L., Kristiansson, K., Kristiansson, P., 1999. Geogas prospecting — an ideal industrial application of PIXE. Nucl. Inst. Methods Phys. Res. B 150, 484–490.

Morner, N.A., Etiope, G., 2002. Carbon degassing from the lithosphere. Glob. Planet. Chang. 33, 185–203.

Patrick, J.W., 1998a. Metallogeny of the McArthur River-Mount Isa-Cloncurry minerals province. Econ. Geol. 93 (8), 1119.

Patrick, J.W., 1998b. An introductionto the metallogeny of the McArthur River-Mount Isa-Cloncurry minerals province. Econ. Geol. 93 (8), 1120–1131.

Pauwels, H., Baubron, J.C., Freyssinet, P., Chensneau, M., 1999. Sorption of metallic compounds on activated carbon: application to exploration for concealed deposits in southern Spain. J. Geochem. Explor. 66, 116–133.

Peng, R.M., Zhai, Y.S., 2004. Hydrothermal mineralization on the Mesoproterozoic passive continental margins of China: a case study of the Langshan-Zha'ertaishan Belt, Inner Mongolia, China. Acta Geol. Sin. Engl. Ed. 78, 534–547.

Peng, R.M., Zhai, Y.S., Han, X.F., Wang, J.P., Qin, J.W., 2007. Magmatic hydrothermal overprinting in the Mesoproterozoic Dongshengmiao deposit, Inner Mongolia: geological and fluid inclusion evidences. Acta Petrol. Sin. 23 (1), 145–152.

Perkins, W.G., Bell, T.H., 1998. Stratiform replacement lead–zinc deposits: a comparison between Mount Isa, Hilton, and McArthur River. Econ. Geol. 93 (8), 1190–1212.

Tong, C.H., Li, J.C., 1999. A new method searching for concealed mineral resources: geogas prospecting based on nuclear analysis and accumulation sampling. J. China Univ. Geosci. 10, 329–332.

Tong, C.H., Li, J.C., Ge, L.Q., Yang, F.G., 1998. Experimental observation of the nano-scale particles in geogas matters and its geological significance. Sci. China Ser. D 41, 325–329.

Wang, X.Q., 2003. Delineation of geochemical blocks for undiscovered large ore deposits using deep-penetrating methods in alluvial terrains of eastern China. J. Geochem. Explor. 77, 15–24.

Wang, X.Q., Cheng, Z.Z., Lu, Y.X., Xu, L., Xie, X.J., 1997. Nanoscale metals in earthgas and mobile forms of metals in overburden in wide-spaced regional exploration for giant deposits in overburden terrains. J. Geochem. Explor. 58, 63–72.

Wang, X.Q., Xie, X.J., Cheng, Z.Z., Liu, D.W., 1999. Delineation of regional geochemical anomalies penetrating through thick cover in concealed terrains — a case history from the Olympic Dam deposit, Australia. J. Geochem. Explor. 66, 85–97.

Wang, X.Q., Wen, X.Q., Ye, R., Liu, Z.Y., Sun, B.B., Zhao, S.Z., Shi, S.J., Wei, H.L., 2007. Vertical variation and dispersion of elements in arid desert regolith: a case study from the Jinwozi gold deposit, northwestern China. Geochem. Explor. Environ. Anal. 7 (2), 163.

Wang, X.Q., Zhang, B.M., Liu, X.M., 2012. Nanogeochemistry: deep-penetrating geochemical exploration through cover. Earth Sci. Front. 19, 101–112 (in Chinese with English abstract).

Wei, X.J., Cao, J.J., Holub, R.F., Hopke, P.K., Zhao, S.J., 2013. TEM study of geogas-transported nanoparticles from the Fankou lead–zinc deposit, Guangdong Province, South China. J. Geochem. Explor. 128, 124–135.

Xia, X.H., 1992. Characteristics and formation conditions of sphalerite in the Dongshengmiao polymetallic pyrite deposit. Acta Petrol. Mineral. 4 (11), 375–382 (in Chinese with English abstract).

Xie, X.J., 1995. Surficial and superimposed geochemical expressions for giant ore deposits. CLARK AH. Giant Ore Deposits II. Queen University Press, Kingston, Canada, pp. 475–485.

Xie, X.J., Wang, X.Q., Xu, L., 1999. Orientation study of strategic deep penetration geochemical methods in the central Kyzylkum desert terrain, Uzbekistan. J. Geochem. Explor. 66, 135–143.

Ye, R., Wang, X.Q., Zhang, B.M., 2014. Microscopic and nanoscale understanding of formation of gold geochemical provinces. Acta Geol. Sin. (Engl. Ed.) 88 (3), 801–809.

Zhang, Z.B., Li, J.H., Huang, C.Y., Liu, H., Zhao, Y.H., 2010. Study on genesis and ore prospecting of Dongshengmiao deposit in Inner Mongolia. J. Jilin Univ. (Earth Sci. Ed.) 40 (4), 791–800 (in Chinese with English abstract).

Zhou, Z.Y., Tao, S., Xu, F.L., Dawson, R., 2003. A physical–mathematical model for the transport of heavy metals and toxic matter from point sources by geogas microbubbles. Ecol. Model. 161, 139–149.